

**LIDAR MEASUREMENTS OF STRATOSPHERIC AEROSOLS  
OVER MENLO PARK, CALIFORNIA;  
OCTOBER 1972-MARCH 1974**

*Prepared by*

PHILIP B. RUSSELL, WILLIAM VIEZEE,  
and RICHARD D. HAKE  
STANFORD RESEARCH INSTITUTE  
MENLO PARK, CALIFORNIA 94025

*June 1974*

Distribution of this report is provided in the interest of information exchange. Responsibility for the contents resides in the author or organization that prepared it.

*Supported by*

CIAP OFFICE  
U.S. DEPARTMENT OF TRANSPORTATION  
WASHINGTON, D.C. 20590

Prepared under Contract NAS2-7261

*for*

AMES RESEARCH CENTER  
NATIONAL AERONAUTICS AND SPACE ADMINISTRATION  
MOFFETT FIELD, CALIFORNIA 94035

**STANFORD RESEARCH INSTITUTE**  
Menlo Park, California 94025 · U.S.A.

Reproduced by  
**NATIONAL TECHNICAL  
INFORMATION SERVICE**  
U.S. Department of Commerce  
Springfield, VA. 22151

**PRICES SUBJECT TO CHANGE**

2mif  
(NASA-CR-137532) LIDAR MEASUREMENTS OF  
STRATOSPHERIC AEROSOLS OVER MENLO PARK,  
CALIFORNIA, OCTOBER 1972 - MARCH 1974  
Final Report (Stanford Research Inst.)  
98 p HC  
95P  
CSCL 04A G3/13 Unclas  
42951  
N74-28888





STANFORD RESEARCH INSTITUTE  
Menlo Park, California 94025 - U.S.A.

Final Report

CR 137532

June 1974

# LIDAR MEASUREMENTS OF STRATOSPHERIC AEROSOLS OVER MENLO PARK, CALIFORNIA; OCTOBER 1972-MARCH 1974

*Prepared by*

PHILIP B. RUSSELL, WILLIAM VIEZEE,  
and RICHARD D. HAKE  
STANFORD RESEARCH INSTITUTE  
MENLO PARK, CALIFORNIA 94025

*Supported by*

CIAP OFFICE  
U.S. DEPARTMENT OF TRANSPORTATION  
WASHINGTON, D.C. 20590

Prepared under Contract NAS2-7261

SRI Project 2217

*Approved by*

R. T. H. COLLIS  
RAY LEADABRAND

*for*

AMES RESEARCH CENTER  
NATIONAL AERONAUTICS AND SPACE ADMINISTRATION  
MOFFETT FIELD, CALIFORNIA 94035

## CONTENTS

LIST OF ILLUSTRATIONS . . . . .	v
LIST OF TABLES . . . . .	vii
SUMMARY . . . . .	ix
ACKNOWLEDGMENTS . . . . .	xiii
1. INTRODUCTION . . . . .	1
2. INSTRUMENTATION AND DATA COLLECTION . . . . .	5
3. METHOD OF DATA ANALYSIS . . . . .	13
4. RESULTS . . . . .	19
(a) Profiles of scattering ratio and particulate backscattering coefficient . . . . .	19
(b) Relation to winds and sudden stratospheric warming . .	29
(c) Particulate optical depths . . . . .	34
(d) Sequential ruby and dye lidar observations . . . . .	40
(e) Comparative lidar/direct-sampling experiments . . . . .	43
(i) WB-57F Overflight . . . . .	44
(ii) Convair 990 Overflight . . . . .	53
(iii) U-2 Overflight . . . . .	63
5. DISCUSSION OF ATMOSPHERIC OBSERVATIONS . . . . .	65
6. NOTES AND RECOMMENDATIONS ON THE LIDAR OBSERVATIONAL TECHNIQUE . . . . .	75

# ILLUSTRATIONS

1	Schematic Diagram of Stratospheric Lidar . . . . .	5
2	Data Sample Showing the Three Principal Steps in the Analysis of the Recorded Lidar Backscatter Measurements . . . . .	15
3	Time Series of Scattering Ratio as a Function of Height, Derived from Lidar Backscatter Observations ( $\lambda = 0.69 \mu\text{m}$ ) Made at Menlo Park, California . . . . .	21
4	Time Series of Particulate Backscattering Coefficient as a Function of Height, Derived from Lidar Backscatter Observations ( $\lambda = 0.69 \mu\text{m}$ ) Made at Menlo Park, California . . . . .	25
5	Time Variability of Layer-Averaged Particulate Backscattering Coefficient (Solid Line) and Zonal Wind (Dashed Line) for Four Altitude Regions . . . . .	30
6	Time Variability of Particulate Optical Thickness for Several Altitude Regions . . . . .	37
7	Comparison of Lidar Profiles Measured with Ruby Transmitter ( $\lambda = 0.6943 \mu\text{m}$ , 2203-2258 PDT) and Dye Transmitter ( $\lambda = 0.5890$ $\mu\text{m}$ , 0130-0419 PDT) at Menlo Park, California, on 15-16 May 1973 . . . . .	42
8	Comparison of Lidar-Measured Particulate Backscattering Coefficients with Computed Value Based on Aircraft Mass Sampler Measurement . . . . .	48
9	Dependence of Lidar- and Aircraft-inferred Particulate Mass Concentration on Assumed Acid Fraction of Sulfuric Acid- Water Solution . . . . .	54
10	Molecular Density Profiles Obtained by Oakland Radiosonde Soundings, Night of 21-22 January 1974 . . . . .	56
11	Profiles of Scattering Ratio Observed by Lidar on Night of 21-22 January 1974 . . . . .	60

PRECEDING PAGE BLANK NOT FILMED

TABLES

1.	Lidar System Parameters . . . . .	6
2.	Lidar Observations Made in this Study . . . . .	20
3.	Light-Scattering and Other Properties Computed for Selected Aerosol Size Distributions and Refractive Indices . .	35
4.	Comparison of Lidar Observations with WB-57F Aircraft Mass Sampling Measurement . . . . .	45
5.	Refractive Index of Sulfuric Acid-Water Solutions for Visible Wavelengths . . . . .	49
6.	Computation of Scattering Ratios from Convair 990 Particle Number Data . . . . .	55

## PRECEDING PAGE BLANK NOT FILMED

### SUMMARY

During an 18-month period, 30 nighttime observations of stratospheric aerosols were made using a ground-based ruby lidar located near the Pacific coast of central California (37.5°N, 122.2°W). Vertical profiles of the lidar scattering ratio and the particulate backscattering coefficient were obtained by reference to a layer of assumed negligible particulate content. An aerosol layer centered near 21 km was clearly evident in all observations, but its magnitude and vertical distribution varied considerably throughout the observation period. A reduction of particulate backscattering in the 23- to 30-km layer during late January 1973 appears to have been associated with the sudden stratospheric warming which occurred at that time.

Typically, a relative minimum in the ratio of particulate to molecular backscattering coefficients was observed near, but not necessarily at, the local tropopause. The maximum, or peak, value of this ratio at the ruby wavelength ( $\lambda = 0.694 \mu\text{m}$ ) typically varied between 0.07 and 0.20. These values indicate a significant decrease in stratospheric particulate backscattering since the lidar observations made by several groups in 1964-65, closely following the Agung volcanic eruption. By using a model backscattering phase function, the lidar measurements were converted to stratospheric particulate optical thicknesses, yielding

values which varied between 0.002 and 0.005 (when converted to a wavelength of 0.55  $\mu\text{m}$ ). These values are smaller by a factor of 5 to 12 than that obtained by searchlight measurements made in 1964-65. The decline in particulate backscattering and optical thickness is shown to be in accord with a time series of measurements made by a number of other methods, including twilight photometry, balloonborne particle counting, and chemical and isotopic analysis of collected particles. Together the results confirm that periodic strong volcanic eruptions have a major effect on the stratospheric aerosol.

During one observation, measurements were made at two wavelengths (0.694 and 0.589  $\mu\text{m}$ ) by sequentially using both a ruby and a dye laser transmitter. The observed wavelength dependence of particulate backscattering was in accord with that expected from previous indications of the particle size distribution of the stratospheric aerosol.

On three occasions aircraft sampling flights were made over the lidar site in connection with lidar observations. Comparative analysis of the lidar and aircraft measurements is presented for two of these overflights. For the first overflight, lidar- and aircraft-inferred ambient particulate mass concentrations at the 18.7-km level are shown to agree by modeling the sampled particles as homogeneous spheres of 75 percent sulfuric acid and 25 percent water, having the Deirmendjian haze H size distribution. The model composition and size distribution are shown to be in accord with chemical analysis of the sampled particles

and several previous results. The second overflight revealed a region of negligible particulate content near the tropopause ( $\approx 9$  to 13 km). This is in accord with the minimum in scattering ratio typically observed in that region. Together the lidar/aircraft comparison experiments provide support for the "matching method" of lidar analysis, which assumes a layer of negligible particulate backscattering within the altitude region over which the lidar signal is analyzed.

We conclude that lidar observations are valuable sources of information on the stratospheric aerosol, and are of special value in extending and complementing available in situ measurements. Without the necessity of converting the raw optical data to physical parameters, the lidar observations reveal the presence, altitude-dependence, backscattering strength, and variability (in space and time) of stratospheric aerosol layers. In many cases this information alone is very useful, and lidar measurements can provide it with a coverage in space and time that would be extremely expensive to achieve with direct sensors. When, on the other hand, data on such physical parameters as particle mass or number density are required, the lidar data can still be of value, both in providing physical parameters by means of tested conversion factors, and also in selecting optimum times and locations for using direct sensors. Stratospheric lidar observations should be enhanced by the addition of multiwavelength techniques and Raman scattering measurements of molecular density profiles.

Thus, in addition to contributing to the data base used to establish the synoptic variability of the stratospheric aerosol, the current study provides information on many of the difficulties inherent in the lidar technique. With greater understanding of these difficulties, the role of the lidar in stratospheric observations becomes more well defined, and continues to be a valuable one.

## ACKNOWLEDGMENTS

The authors appreciate and gratefully acknowledge the guidance of R.T.H. Collis in directing this research program. Discussions with R. Penndorf, N. Farlow, G. Ferry, W. Sedlacek, and A. Anderson provided valuable assistance. In addition we are grateful to W. Sedlacek, A. Lazrus, B. Gandrud, D. Briehl, and G. Ferry for releasing their particle analysis data prior to publication. The stratospheric wind data were supplied through the courtesy of the Pacific Missile Range, Point Mugu, California. J. W. Knotts and J. Van der Laan were instrumental in obtaining the lidar data profiles. A. Burris and R. Hadfield provided valuable assistance in presenting and analyzing the data. We gratefully acknowledge the perseverance of M. Kucinski and N. Craig in typing the manuscript. This research was supported by the CIAP Office of the U.S. Department of Transportation (through NASA Ames Research Center, Contract NAS2-7261) and SRI internal research funds.

## 1. INTRODUCTION

The presence of optically significant amounts of particulate material in the stratosphere was deduced nearly a century ago on the basis of the color of the twilight sky, together with the awesome demonstration by the Krakotoa eruption in 1883 that volcanic ejecta could indeed be propelled into the stratosphere. Since the early twilight observations of Gruner and Kleinert (1927), the presence of stratospheric aerosol layers has been confirmed, and their properties studied, by a variety of direct sampling and remote observation techniques. These techniques--which include collection by impactors and filters, particle counting by balloon-borne photoelectric detectors, rocket- and aircraft-borne sky photometry, balloon-borne solar aureole photometry, as well as ground-based twilight sky photometry and searchlight scattering measurements--have produced a wealth of information and a rather extensive literature, which has been summarized and reviewed by Grams and Fiocco (1967), Rosen (1969), Reiter (1971), Cadle (1972), and Castleman (1974), among others. In addition to the field measurements, laboratory investigations, as for example by Bigg et al. (1971), Farlow et al. (1973), and Friend et al. (1973), have contributed supplementary information on the chemical composition and formation mechanisms of stratospheric aerosols.

From these investigations a general picture has emerged of a broad maximum in stratospheric particulate concentration (the so-called "Junge" layer) centered at an altitude of approximately 20 km, with occasional appearances of higher layers. The single most abundant constituent of the particles is sulfate, existing primarily as sulfuric acid and ammonium sulfate. The particles evidently form locally from sulfur-bearing gases (e.g., sulfur dioxide and hydrogen sulfide) entering from the troposphere through the tropical Hadley cell circulation, with major perturbations from occasional volcanic activity (Castleman et al., 1973a,b). Less often, the layer may be enhanced by extraterrestrial material, for example at times of meteoric influx.

During the past decade, the lidar, or laser radar, has been added to the list of remote-sensing instruments that have proven useful in studies of the stratospheric aerosol. (For a review of laser radar applications in the upper atmosphere, see Kent and Wright, 1970.) In applying the lidar technique to stratospheric studies, a pulsed laser beam is projected vertically into the atmosphere, and the energy scattered back by stratospheric gases and particles is measured as a function of altitude. Differences between the observed return signal and that expected from a purely gaseous atmosphere are indicative of the presence of particulate matter. Since the pioneering observations by Fiocco and Grams (1964) (see also Grams 1966; Grams and Fiocco 1967) and Collis and Lidga (1966), this technique has been employed to observe the layered

structure of the stratospheric aerosol from ground-based sites in Massachusetts, Colorado, California, Alaska, Jamaica, Japan, Brazil, Australia, the Soviet Union, and Israel (Fiocco and Grams 1966; Clemesha et al., 1966; Kent et al., 1967; Phillipowskyj et al., 1968; Schuster 1970; Clemesha and Rodrigues 1971; Bartusek et al., 1970; Ottway 1972; Hirono et al., 1972; Zakharov et al., 1973; Cohen and Graber 1973).

In August and September of 1971, Fox et al. (1973) extended the lidar observations of the stratosphere by using an airborne laser radar system to obtain measurements on extensive flights over the Pacific and Atlantic Oceans. In presenting their results, Fox et al. also summarize a number of stratospheric lidar observations made prior to their investigation. Taken together, the observations reveal a decreasing trend in stratospheric particulate backscattering over the period 1964 to late 1971. This decline is shown to be in accord with other remote and in-situ measurements, particularly the twilight photometry of Volz (1969, 1970, 1972), which had indicated a large increase in stratospheric aerosol concentration following the eruption of the volcano Agung on Bali in March 1963. As noted by Cronin (1971), Casteleman (1974), and others, volcanic eruptions subsequent to the Agung event may have partially replenished the Junge layer concentration, but evidently not enough to cancel this general decline.

Interest in the composition and dynamics of the stratosphere has recently been intensified by concern that the stratosphere could be

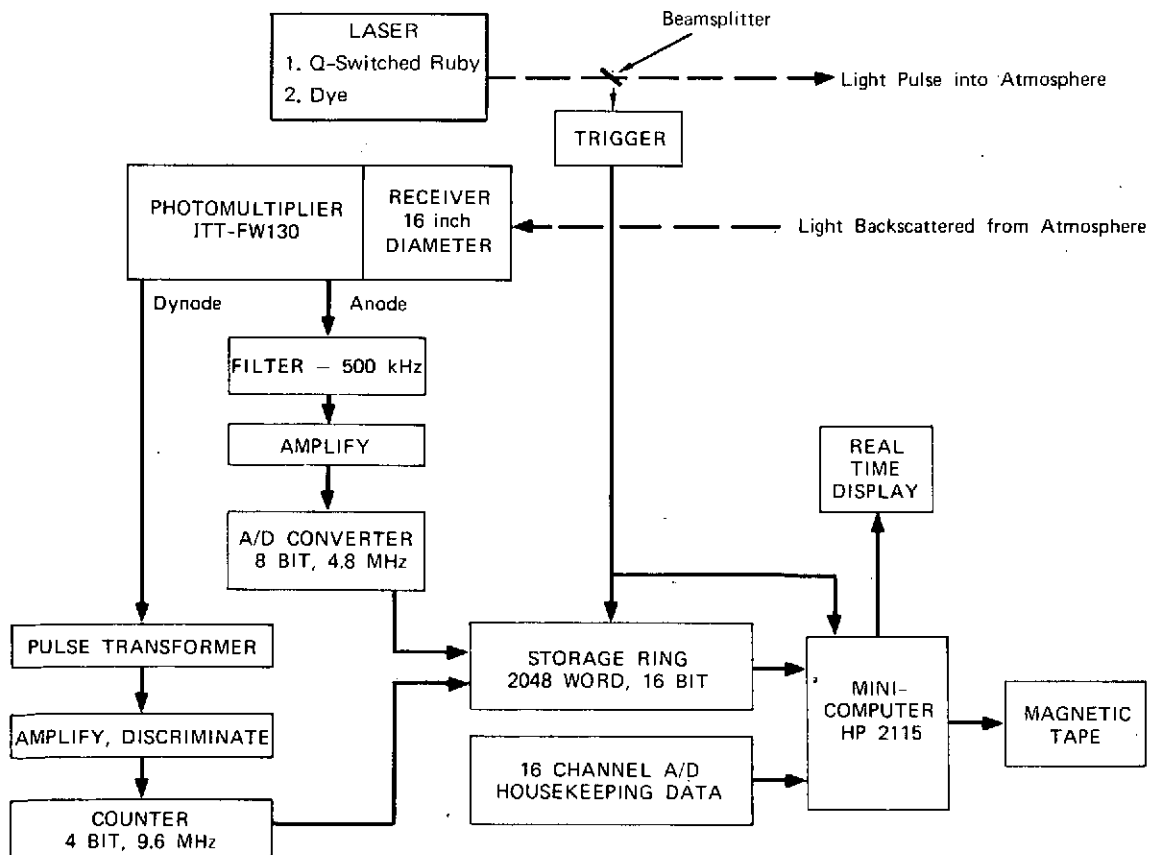
significantly modified by the exhaust emissions of aircraft and other aerospace vehicles, with possibly severe effects on the climate at the earth's surface. This concern led to the formation in 1971 of a major stratospheric research study, the Climatic Impact Assessment Program (CIAP), funded by the U.S. Department of Transportation. In considering the possibility of climatic change, the particulate phase of the stratosphere is of considerable interest, not only because of its direct effect on the transfer of solar radiation, but also because of its possibly important role in stratospheric photochemical processes, and its ability to serve as a tracer of stratospheric transport. Therefore, CIAP has funded a number of studies of the stratospheric aerosol, including three that use lidar techniques.

This paper describes the results of one of these studies, conducted at the Stanford Research Institute in Menlo Park, California ( $37.5^{\circ}\text{N}$ ,  $122.2^{\circ}\text{W}$ ), over the 18-month period from October 1972 to March 1974. The objectives of the study were twofold: first, to provide a record, or climatology, of the temporal and (vertical) spatial variability of particulate material in the natural (unperturbed) stratosphere above the lidar site; and second, to provide comparative data on the stratospheric aerosol by conducting coordinated observations employing the lidar and other, direct sensors to make joint observations. Results of this and other CIAP-sponsored investigations of the stratosphere will be published in the extensive monograph, The Natural Stratosphere, to appear in late 1974 or 1975.

## 2. INSTRUMENTATION AND DATA COLLECTION

### (a) Lidar System

A schematic diagram of the laser radar system used in this study is shown in Fig. 1. For descriptive purposes it may be conveniently divided into transmitter and receiver portions. The characteristics of these two portions of the system are summarized in Table 1. The dye transmitter was used for only one of the observations reported herein.



SA-2217-25

FIGURE 1 SCHEMATIC DIAGRAM OF STRATOSPHERIC LIDAR

Table 1

## LIDAR SYSTEM PARAMETERS

Equipment	Parameters
Ruby transmitter	
Wavelength	694.3 nm
Energy per pulse	1-2 Joules
Pulse duration	< 30 ns (q-switched)
Pulse frequency	0.5 Hz (1 pulse every 2 seconds)
Beam diameter	15.2 cm (expanded)
Beam divergence	0.5 mrad (full angle)
Dye transmitter	
Wavelength	589.0 nm
Energy per pulse	100-150 mJ
Pulse duration	300 ns
Pulse frequency	0.25 Hz (1 pulse every 4 seconds)
Beam diameter	12.7 cm
Beam divergence	0.5 mrad (full angle)
Receiver	
Diameter	40.6 cm (Cassegrain)
Unobscured area	1070 cm <sup>2</sup>
Acceptance cone	2 mrad (full angle)
Filter bandwidth	1.0 nm
Filter transmission	50%
Separation from laser	7 m
Beam overlap	height > 8 km

The ruby transmitter consisted of a high-energy ruby laser, Korad K15Q, q-switched with a passive dye cell. The laser produced 1- to 2-joule pulses of  $\leq 30$ -ns duration at a rate of 0.5 Hz or less. The 1.4 cm diameter beam from the ruby rod was expanded to 15.2 cm and at the same time collimated to 0.5-mrad divergence before being transmitted vertically into the atmosphere. A portion of the beam was diverted into a detector

for supplying a master trigger pulse to the rest of the system. In addition to starting the data acquisition cycle, this pulse served as the timing event for range determination.

When the dye laser was used in place of the ruby laser, the energy output was 100 to 150 mJ per pulse at the wavelength of  $\sim 589$  nm. Other characteristics of the dye system are summarized in Table 1.

Light backscattered from the atmosphere was collected by a 40.6 cm Cassegrainian telescope and focused (through a 1-nm interference filter for background rejection) onto an ITT-FW130 photomultiplier tube (PMT). The receiving telescope was displaced horizontally roughly 7 m from the vertical axis of the transmitted laser beam. This displacement eliminated problems due to fluorescence of the ruby rod (making a shutter unnecessary), but did make the convergence of the transmitting and receiving beams more difficult. It also meant that full convergence could not be achieved below 10 km if convergence were to be maintained at all higher altitudes with an optimally narrow receiver beamwidth.

Two outputs were taken from the PMT. The signal from the last dynode was fed through a pulse transformer into a three-stage amplifier and discriminator, and then into a 4-bit counter sampled at 9.6 MHz. Two 4-bit counter words were combined in parallel and stored in one half of the 16-bit word of the storage ring at a 4.8-MHz rate.

Simultaneously, the anode signal of the PMT was fed through a 500-KHz filter into a high-linearity amplifier and then into an 8-bit

analog-to-digital converter. (Logarithmic amplifiers were not consistent with the required 1 percent accuracy.) The output of the converter was then clocked into the ring at the 4.8-MHz rate. The frequency rolloff of the filter was consistent with the range resolution (0.25 to 0.33 km) desired. The counter signal was useful at high altitudes where the photon arrival rate was low enough that the individual PMT pulses were not run together. At lower altitudes where the pulses could not be resolved individually, the signal was strong enough that the analog signal could be accurately digitized.

The sampling rate of 4.8 MHz gave 32 samples per kilometer (65 per kilometer for the counter), and the 2048-word storage ring could accommodate 64 km of data. After the ring had been filled, it was read into an HP 2115 minicomputer along with relevant housekeeping data, and from there was put in packed form on 12.7-cm magnetic tape for later analysis. The data were also displayed in real time to make certain the system was operating correctly.

Two major changes were implemented in the system during the measurement series described herein. In mid-December 1972 a new ruby rod was installed in the laser, allowing the pulse repetition rate to be increased and also giving more energy per pulse. In mid-January 1973 the receiver optical system was changed from focusing the sky onto the PMT face to focusing the telescope aperture onto the PMT. This change eliminated the problem of large-scale systematic errors due to irregularities in the

photo-cathode sensitivity that had prohibited most earlier runs from being useful below 20 km.

(b) Treatment of data profiles

The first stage in data analysis was done on an SDS-930 computer. The tape was unpacked, pulse by pulse, and the return signal from each laser pulse was examined to ascertain that the energy in the pulse was within certain bounds and that double-pulsing did not occur. Since the passive-dye q-switch was not 100 percent effective in generating only a single pulse per flash, it was necessary to screen the transmitted pulses by computer to eliminate multiple pulses. The effect of multiple pulsing was sufficiently obvious that all multiple pulses could be eliminated by demanding that the shape of the backscatter profile be within certain broad bounds that were programmed into the computer. The return signals from all acceptable pulses were summed together in 0.25-km range bins, then range-corrected, and written on another tape for the final analysis stage.

The linearity of the system was initially established and then periodically checked by summing all low-power pulses and all high-power pulses and making certain that the range-dependence of the return signal was identical for the two power levels. This procedure assured that the receiver system was linear and that there were no power-dependent effects in the transmitter. A further check was provided by noting the consistency between the analog return signal and the counter signal at

high altitudes where the counter was free of pulse-pair resolution difficulties.

The exponential decrease in atmospheric density with height, together with the  $1/R^2$  geometrical dependence of the received lidar power, produces an extremely rapid decrease in PMT output signal with increasing time after pulse transmission. This rapid change in photomultiplier output limits the altitude range over which the linear anode signal can be accurately digitized into 8-bit words. In several previous lidar systems (see, e.g., Schuster 1970; Fox et al., 1973; Spinhirne et al., 1973), this digitization problem was countered by using a gain-switching amplifier between the PMT and the analog-to-digital converter. A gain-switching amplifier was not used in the present study because of problems associated with matching the signal before and after the gain-switching transient. For the early observations, which were confined to the altitude range of 13 to 30 km, this did not present a problem, because the signal dynamic range could be adequately spanned by the combination of an 8-bit word and the photon-counting channel. However, observations made after May 1973 extended down to altitudes of 10 km and frequently lower, and the dynamic range of the PMT output exceeded that of the data acquisition system, which was originally constructed for higher altitude observations.

The dynamic range problem was circumvented in the observations made after May 1973 by sequentially operating the lidar in two modes of different sensitivity. In the low-sensitivity mode, a portion of the receiver

telescope aperture was covered and PMT anode signals were accurately digitized in a low-altitude range. The data profile from the counter on the last PMT dynode (which is valid for all altitudes above saturation) was then multiplied by the constant (the relative anode/dynode system calibration) that gave the best (least-square) fit between the anode and dynode profiles in the common altitude region where both profiles were valid. Thus a composite low-sensitivity data profile was constructed, consisting of the digitized anode profile at the lowest altitudes, the average of the anode and counter profiles in the altitude region of mutual validity, and the counter profile above that region. This composite profile is valid (i.e., contains no systematic error) for all altitudes, but of course has increasingly large random photon-counting error at high altitudes due to the reduced receiver area.

Therefore the lidar was also operated in a high-sensitivity mode, with the receiver unobscured, to acquire a composite profile, valid over a higher altitude range, in exactly the same manner. The system was alternately operated in low- and high-sensitivity modes, each for periods of approximately 30 minutes or 400 shots. This alternation procedure was followed so that changes in atmospheric structure on the time scale of one-half to several hours would not be obscured. If no such changes were evident in the data, a "grand composite" profile, representative of the complete period of observation, was then

constructed from the low- and high-sensitivity profiles by fitting them together in the altitude region where both were valid.

The individual anode and counter data profiles for each sensitivity mode were accumulated by the SDS-930 computer as described above. All profile-matching was then accomplished on a CDC 6400 computer, using a linear least-square fitting routine.

### 3. METHOD OF DATA ANALYSIS

It has become standard practice in most stratospheric lidar investigations to use the "scattering ratio"  $R$  as the fundamental form for expressing measurement data. The scattering ratio is defined as

$$R(z) \equiv \frac{f_m(z) + f_p(z)}{f_m(z)} = 1 + \frac{f_p(z)}{f_m(z)}, \quad (1)$$

where  $f_m(z)$  and  $f_p(z)$  are, respectively, the elastic volume backscattering coefficients of the molecular (or gaseous) and particulate phases of the atmosphere, both measured at altitude  $z$ . Expressing the data as a ratio of backscattering coefficients permits them to be presented in a standard format without making any assumptions as to the nature of the particulate matter. Thus the observation of scattering ratios greater than unity in an atmospheric region indicates the presence of particulate matter, and gives its backscattering strength relative to that of local gases, but does not provide more specific information on the nature of the particles. To convert from the volume backscattering coefficient to such physical parameters as particle number or mass requires additional information on the refractive index, size distribution, and shape of the particles.

#### (a) Computation of scattering ratios and particulate backscattering coefficients

In the present study, profiles of the scattering ratio  $R(z)$  were obtained from the lidar signal profiles in the following manner, as

illustrated in Fig. 2 for an actual observation. The measured range-corrected lidar signal profile  $S(z)$ , given by

$$S(z) = K[f_m(z) + f_p(z)] q^2(z) , \quad (2)$$

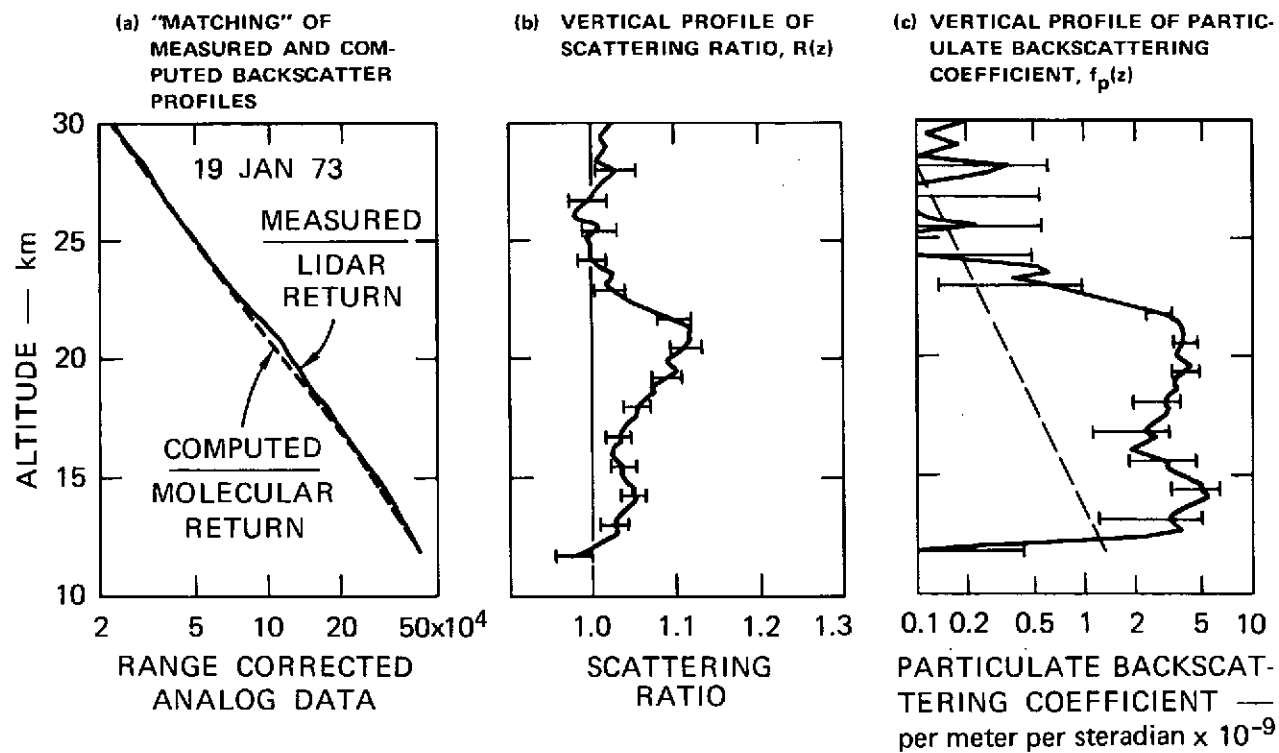
was divided by the computed "molecular" signal profile  $M(z)$ , given by

$$M(z) = Kf_m(z) q^2(z) , \quad (3)$$

thus yielding the ratio

$$R(z) = \frac{S(z)}{M(z)} = \frac{f_m(z) + f_p(z)}{f_m(z)} , \quad (4)$$

in agreement with Eq. (1). In eqs. (2) and (3),  $q^2(z)$  is the two-way optical transmission between altitudes  $z_1$  and  $z$  (where  $z_1$  is the lowest altitude for which the lidar signal is analyzed), and  $K$  is a factor that includes the total transmitted energy, the two-way transmission between the lidar and altitude and  $z_1$ , and also the lidar system calibration constant. In computing  $M(z)$ ,  $f_m(z)$  was obtained from a radiosonde-measured molecular density profile, and  $q^2(z)$  was obtained from a stratospheric extinction model [see Section 4.(c)]. However, because the transmission through low-level haze and cirrus varied from observation to observation, and also because (for this reason) we did not calibrate the lidar, the constant  $K$  was unknown for any given observation.  $K$  was therefore determined by the "matching method," which was first used by Fiocco and Grams



SA-2217-22

FIGURE 2 DATA SAMPLE SHOWING THE THREE PRINCIPAL STEPS IN THE ANALYSIS OF THE RECORDED LIDAR BACKSCATTER MEASUREMENTS

(1964) and which has been adopted (in varying forms) in most subsequent stratospheric lidar studies.

The matching method of data analysis rests upon the fundamental assumption that, at some level  $z_0$  within the altitude region spanned by the lidar signal profile, the particulate content is nil or negligible. Clearly, if such a "clean level" exists, it must have scattering ratio  $R(z_0) = 1$ . Furthermore, this ratio must be the minimum of all ratios in the altitude range analyzed. On this assumption,  $K$  may be determined by first assigning it an arbitrary value (e.g.,  $K = 1$ ), computing the scattering ratio profile using Eq. (4), and then readjusting  $K$  so that the statistically significant minimum value,  $R(z_0)$ , is unity. In other words, the measured and computed profiles,  $S(z)$  and  $M(z)$ , are "matched" together at the level(s) where their ratio is a minimum, as shown in Fig. 2a. The profile of scattering ratio thus obtained is shown in Fig. 2b.

Given the scattering ratio profile, the profile of particulate backscattering coefficient is readily computed from

$$f_p(z) = [R(z) - 1] f_m(z) \quad , \quad (5)$$

as shown in Fig. 2c. [The dashed line is drawn at a constant mixing ratio of  $0.01 f_m(z)$ .] Again, in the present work the molecular backscattering coefficient was obtained from a current radiosonde density profile using

$$f_m(z) = C_R(180^\circ) N_m(z) \quad , \quad (6)$$

where  $C_R(180^\circ) = 2.114 \times 10^{-28} \text{ cm}^2$  is the Rayleigh backscattering cross section of an average air molecule at the ruby wavelength ( $\lambda = 694.3 \text{ nm}$ ), and  $N_m(z)$  is the molecular number density at height  $z$ . The importance of using a measured profile of molecular density, rather than a standard profile, has been discussed in some detail by Russell et al. (1973a). This importance results from the fact that at certain levels (especially near the tropopause) on any given night the actual density profile may differ from the standard by several percent or more, and use of an erroneous density profile results in significant distortions in lidar-derived profiles of scattering ratio and particulate backscattering coefficient.

#### (b) Errors

The error bars shown in Fig. 2 result from three sources of uncertainty: (1) random counting errors in the lidar signal  $S(z)$ ; (2) possible relative errors (between two stratospheric altitudes) in the radiosonde measured density profile  $N_m(z)$ ; and (3) possible differences between the actual stratospheric transmission and the model profile  $q(z)$ . The signal counting error was maintained at two percent or less by summing together 0.25-km altitude bins at the higher altitudes. In accordance with Hoxit and Henry (1973) and Lenhard (1973), we estimated the probable relative radiosonde density error to be one percent. The probable error in the model two-way transmission  $q^2(z)$  was also estimated at one percent

[see further discussion in Section 4.(c)]. All stated errors are  $1\sigma$  (i.e., one standard deviation or standard error). They were combined according to the error-propagation analysis of Viezee et al., 1973a, (see also Collis et al., 1973; Russell et al., 1973a) to give the error bars of  $\pm 1\sigma$  that are shown in Fig. 2.

It is emphasized that the error bars shown in Fig. 2 (and subsequent figures) do not include possible errors associated with the matching method assumption that the lidar profile includes a level with negligible particulate content. If, indeed, the assumed "clean" level in fact contains nonnegligible particulate material, then an error is introduced into the derived profiles. Although the magnitude of this error is difficult to estimate, its sign is always known. That is, if the assumed "clean" level actually contains a significant amount of particulate material, then the derived profiles of  $R(z)$  and  $f_m(z)$  will be too small. Thus the matching method can lead to an underestimate of particulate content, but it cannot lead to an overestimate.

#### 4. RESULTS

In the present study, successful lidar observations were made at Menlo Park, California (37.5°N, 122.2°W) on 30 dates, as listed in Table 2. All observations were made at night to reduce background noise from skylight. Observations could not be made if a layer of clouds (other than thin cirrus) was present, and cloud occurrence thus frequently influenced the choice of observation dates. Occasionally, observations were made to coincide with concurrent direct sampling measurements [see Section 4(e)].

##### (a) Profiles of scattering ratio and particulate backscattering coefficient

Profiles of scattering ratio  $R(z)$  and particulate backscattering coefficient  $f_p(z)$  obtained in each of the observations are shown in Figs. 3 and 4. The presence in all observations of a maximum in scattering ratio between the altitudes of 19 and 25 km confirms the existence of the Junge aerosol layer on all observation dates. The maximum value of the "backscattering mixing ratio" or "scattering excess:"  $R(z)-1$ , varies between 7 percent and 22 percent over the observation period, or by about a factor of three. These values are somewhat larger than those measured by the dye lidar ( $\lambda \approx 585$  nm) of Fox et al. (1973), but agree well with more recent values obtained by the ruby lidars of other CIAP investigators (Dynatrend 1973; Schuster et al., 1973; Melfi et al.,

Table 2

## LIDAR OBSERVATIONS MADE IN THIS STUDY

Date*	Altitude Range (km)	Wavelength (nm)	Number of shots
23 Oct 72	18.5-30.0	694.3	1236
28 Nov 72	20.0-30.0	694.3	1083
30 Nov 72	15.0-27.0	694.3	1136
11 Dec 72	19.0-29.0	694.3	970
4 Jan 73	20.0-30.0	694.3	1633
19 Jan 73	13.0-30.0	694.3	619
22 Jan 73	16.0-30.0	694.3	699
15 Feb 73	16.0-30.0	694.3	398
13 Mar 73	15.0-30.0	694.3	714
22 Mar 73	13.0-30.0	694.3	958
27 Mar 73	12.0-30.0	694.3	1332
2 Apr 73	13.5-30.0	694.3	1639
10 Apr 73	13.0-30.0	694.3	1669
15 May 73	12.5-30.0	694.3	1040
		589	792
11 Jan 73	10.0-30.0	694.3	473
18 Jun 73	10.0-30.0	694.3	1522
5 Jul 73	10.0-30.0	694.3	315
17 Jul 73	10.0-30.0	694.3	681
23 Jul 73	10.0-30.0	694.3	1754
24 Jul 73	10.0-30.0	694.3	1700
26 Jul 73 <sup>†</sup>	10.0-30.0	694.3	1377
9 Aug 73	10.0-30.0	694.3	854
23 Aug 73	10.0-30.0	694.3	1436
11 Sep 73	10.0-30.0	694.3	1065
2 Oct 73	9.0-30.0	694.3	285
9 Oct 73	7.5-30.0	694.3	1817
27 Nov 73	7.7-30.0	694.3	2501
21 Jan 74 <sup>‡</sup>	8.0-30.0	694.3	4412
8 Mar 74	8.0-30.0	694.3	1862
18 Mar 74 <sup>§</sup>	7.0-30.0	694.3	1526

\* If an observation extended through midnight, the date listed is that of the evening, rather than the morning.

<sup>†</sup> WB-57F overflight made on morning prior to the observation.

<sup>‡</sup> Corvair 990 overflight made concurrent with this observation.

<sup>§</sup> CU-2 overflight made concurrent with this observation.

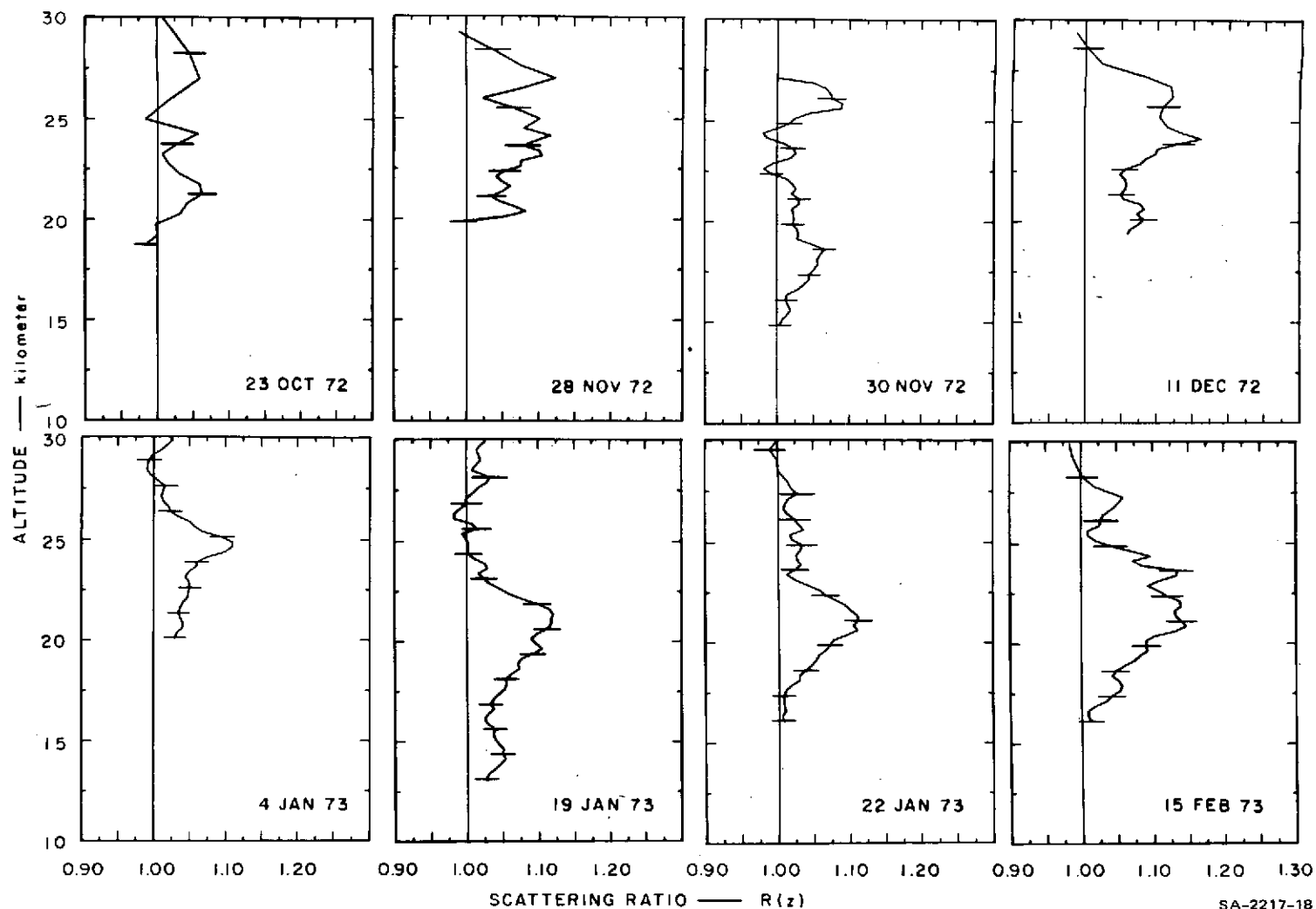
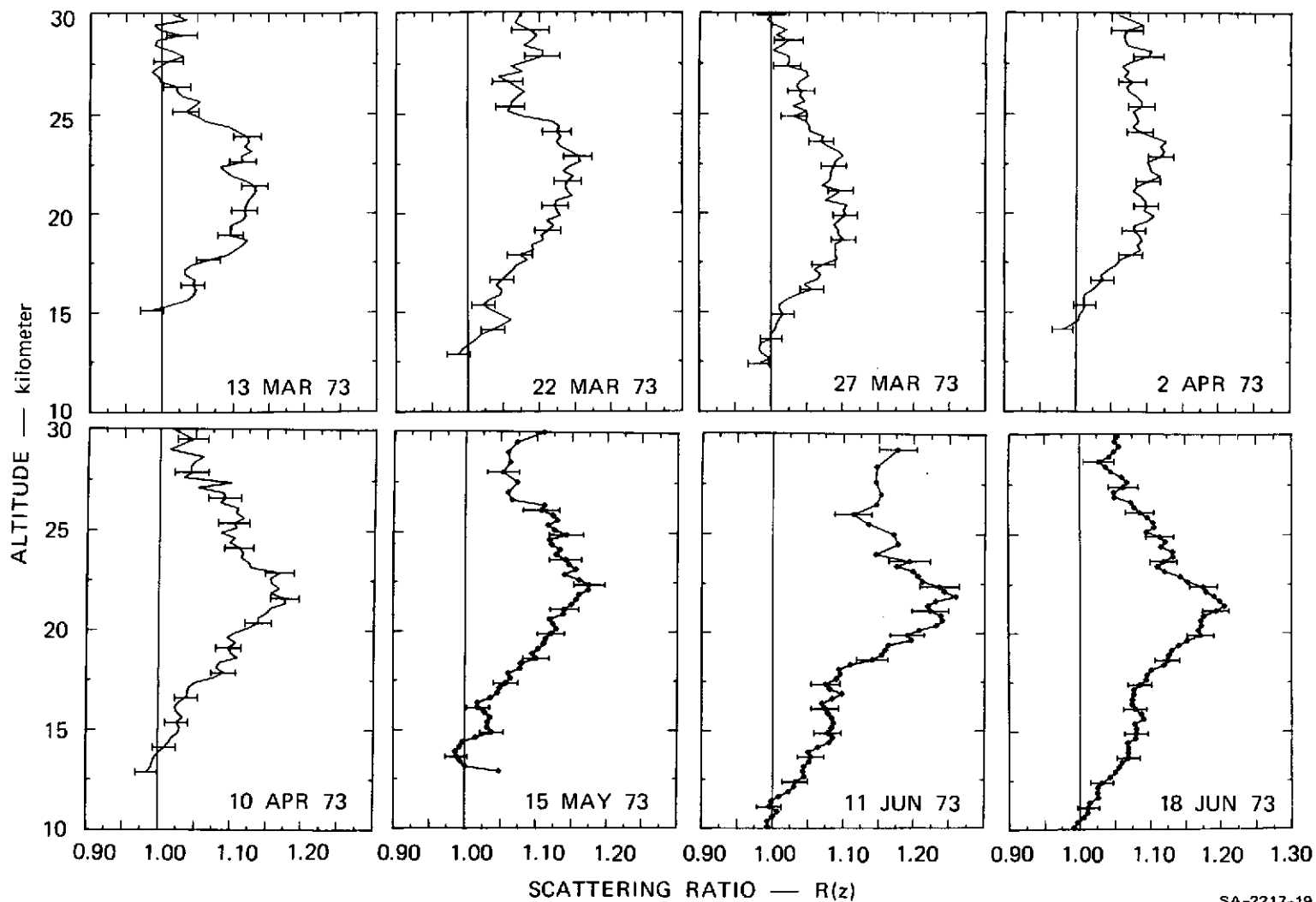


FIGURE 3a TIME SERIES OF SCATTERING RATIO AS A FUNCTION OF HEIGHT, DERIVED FROM LIDAR BACKSCATTER OBSERVATIONS ( $\lambda = 0.69 \mu\text{m}$ ) MADE AT MENLO PARK, CALIFORNIA

Profiles are computed using Oakland radiosonde sounding for molecular densities, and assuming Rayleigh and ozone extinction as given by Elterman (1968), with no particulate extinction. Error bars are  $\pm 1\sigma$  (shown at every fifth data point).

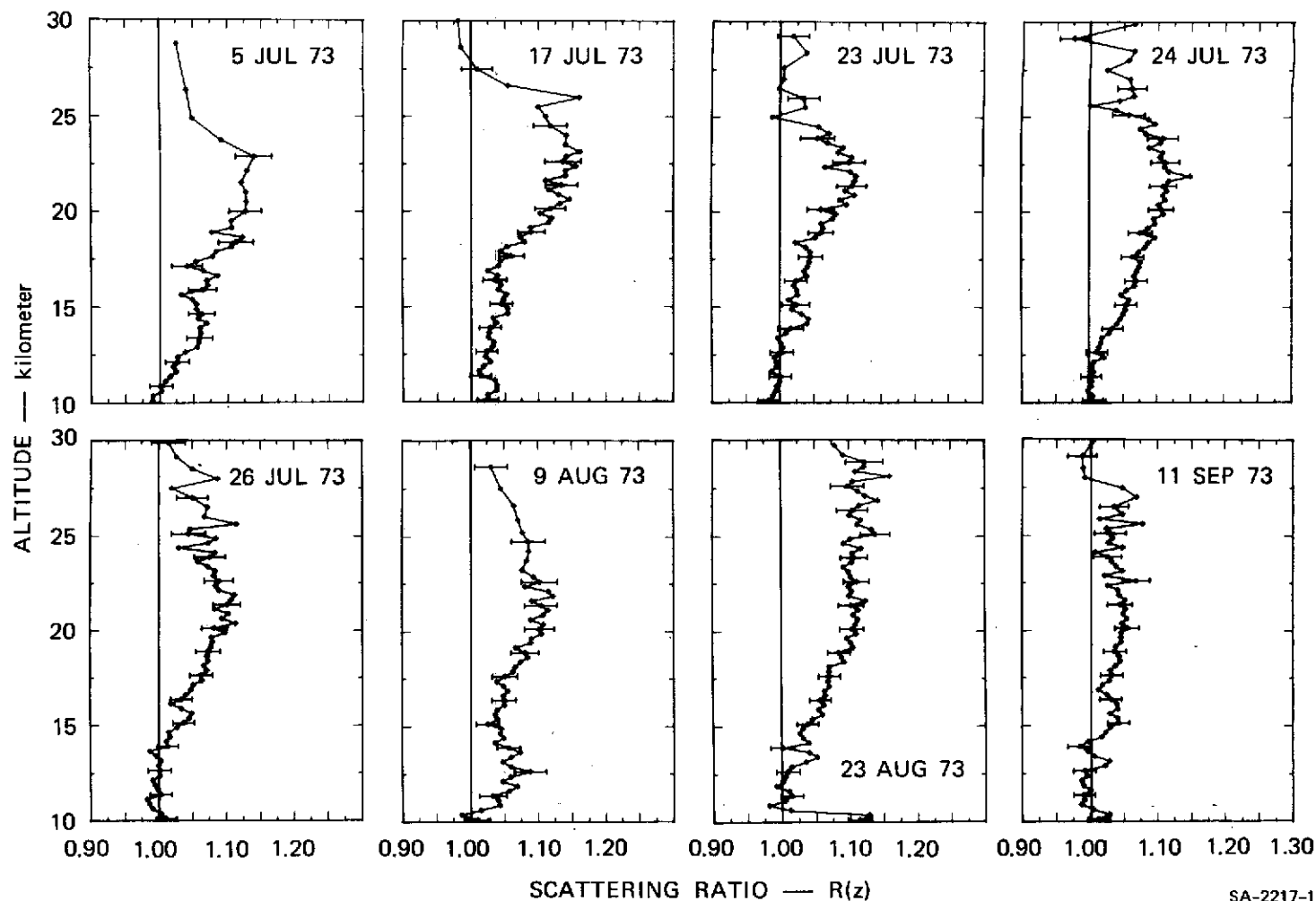
SA-2217-18



SA-2217-19

FIGURE 3b TIME SERIES OF SCATTERING RATIO AS A FUNCTION OF HEIGHT, DERIVED FROM LIDAR BACKSCATTER OBSERVATIONS ( $\lambda = 0.69 \mu\text{m}$ ) MADE AT MENLO PARK, CALIFORNIA (Continued)

Profiles are computed using Oakland radiosonde sounding for molecular densities, and assuming Rayleigh and ozone extinction as given by Elterman (1968), with no particulate extinction. Error bars are  $\pm 1\sigma$  (shown at every fifth data point).



SA-2217-1

FIGURE 3c TIME SERIES OF SCATTERING RATIO AS A FUNCTION OF HEIGHT, DERIVED FROM LIDAR BACKSCATTER OBSERVATIONS ( $\lambda = 0.69 \mu\text{m}$ ) MADE AT MENLO PARK, CALIFORNIA (Continued)

Profiles are computed using Oakland radiosonde sounding for molecular densities, and assuming Rayleigh and ozone extinction as given by Elterman (1968), with no particulate extinction. Error bars are  $\pm 1\sigma$  (shown at every fifth data point).

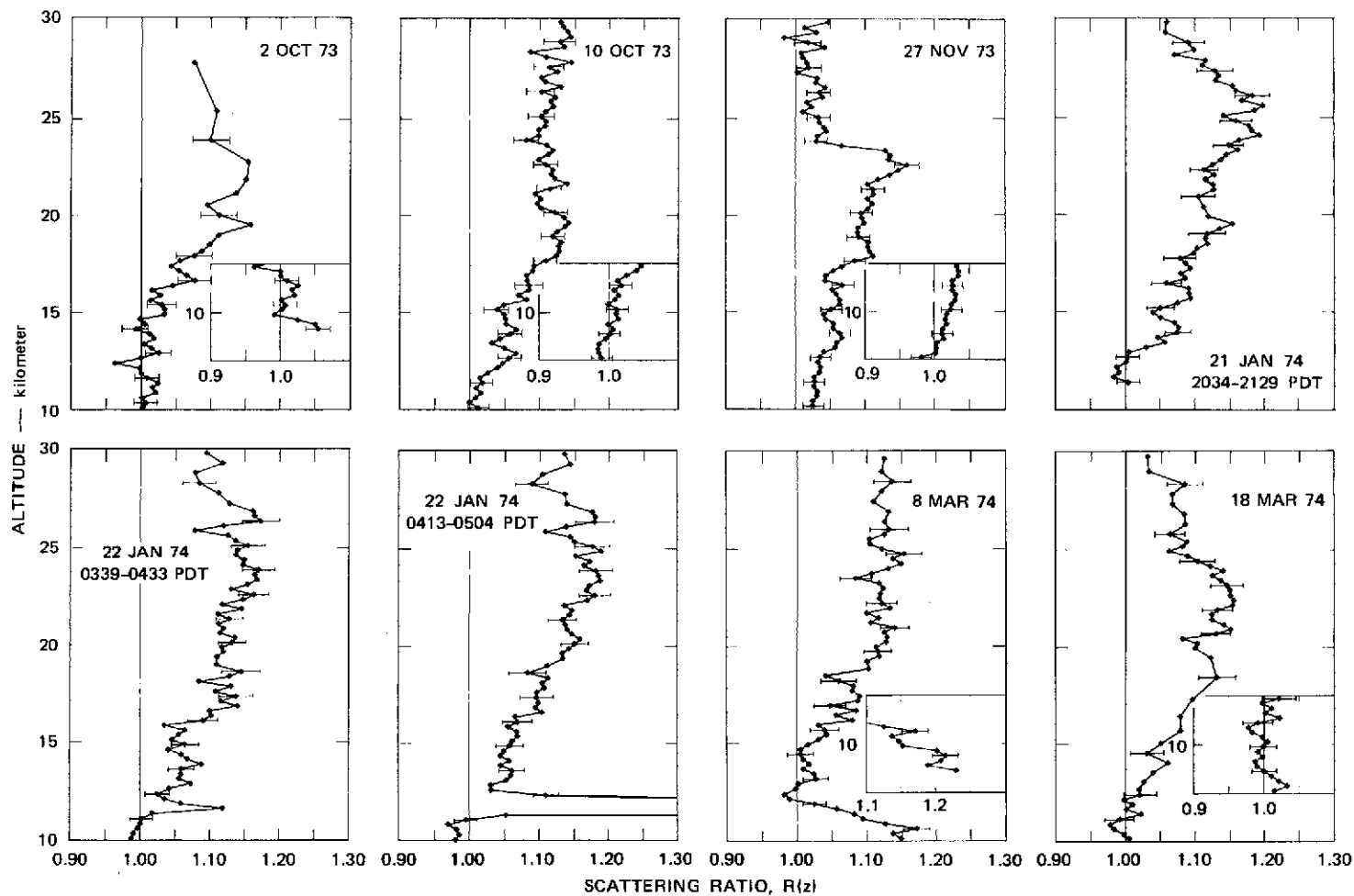


FIGURE 3d TIME SERIES OF SCATTERING RATIO AS A FUNCTION OF HEIGHT, DERIVED FROM LIDAR BACKSCATTER OBSERVATIONS ( $\lambda = 0.69 \mu\text{m}$ ) MADE AT MENLO PARK, CALIFORNIA (Concluded)

Profiles are computed using Oakland radiosonde sounding for molecular densities, and assuming Rayleigh and ozone extinction as given by Elterman (1968), with no particulate extinction. Error bars are  $\pm 1\sigma$  (shown at every fifth data point).

SA-2217-13

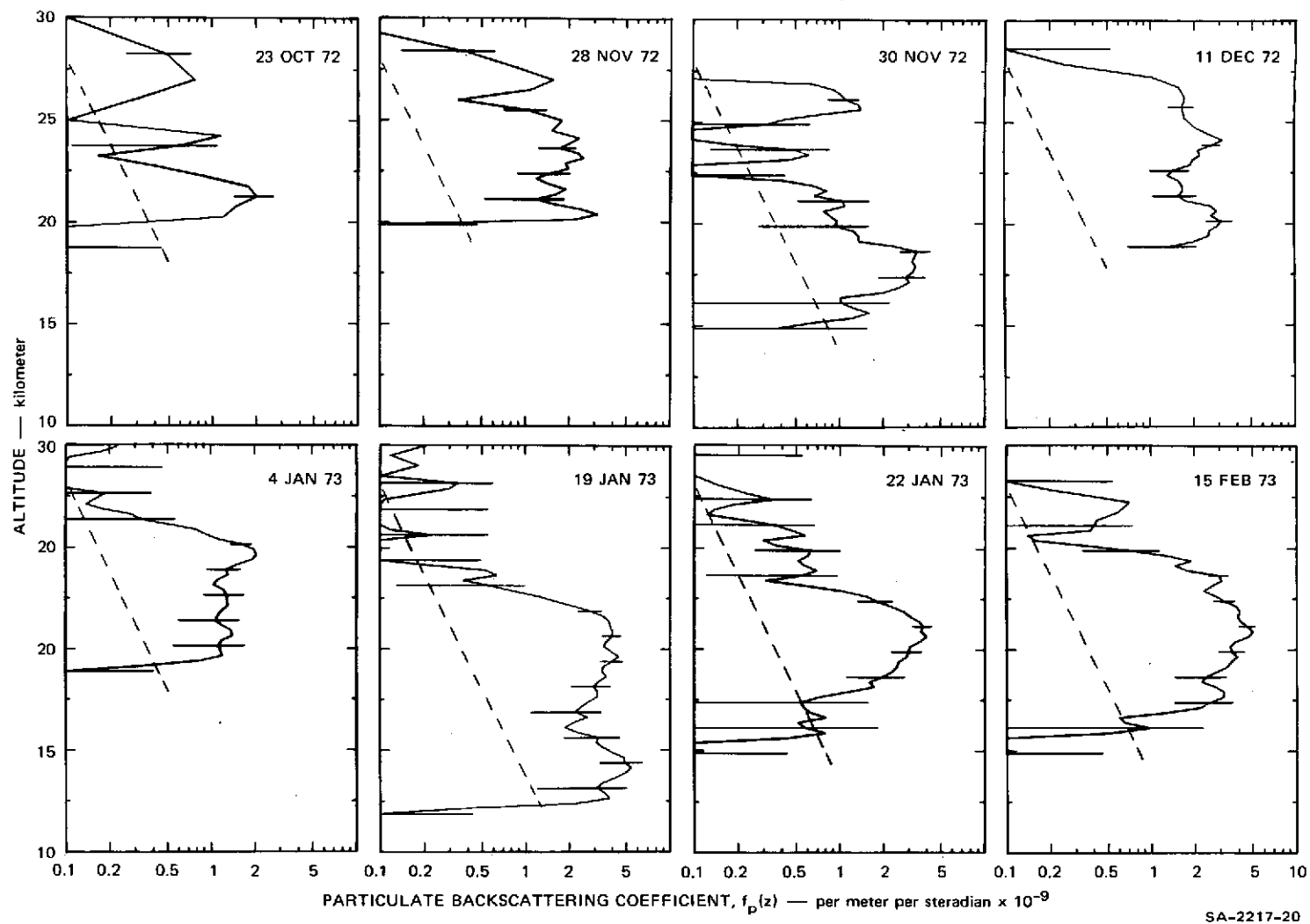


FIGURE 4a TIME SERIES OF PARTICULATE BACKSCATTERING COEFFICIENT AS A FUNCTION OF HEIGHT, DERIVED FROM LIDAR BACKSCATTER OBSERVATIONS ( $\lambda = 0.69 \mu\text{m}$ ) MADE AT MENLO PARK, CALIFORNIA

Profiles are computed using Oakland radiosonde sounding for molecular densities, and assuming Rayleigh and ozone extinction as given by Elterman (1968), with no particulate extinction. Error bars are  $\pm 1\sigma$  (shown at every fifth data point). Dashed line is drawn at a constant mixing ratio of 1% of the molecular backscattering coefficient.

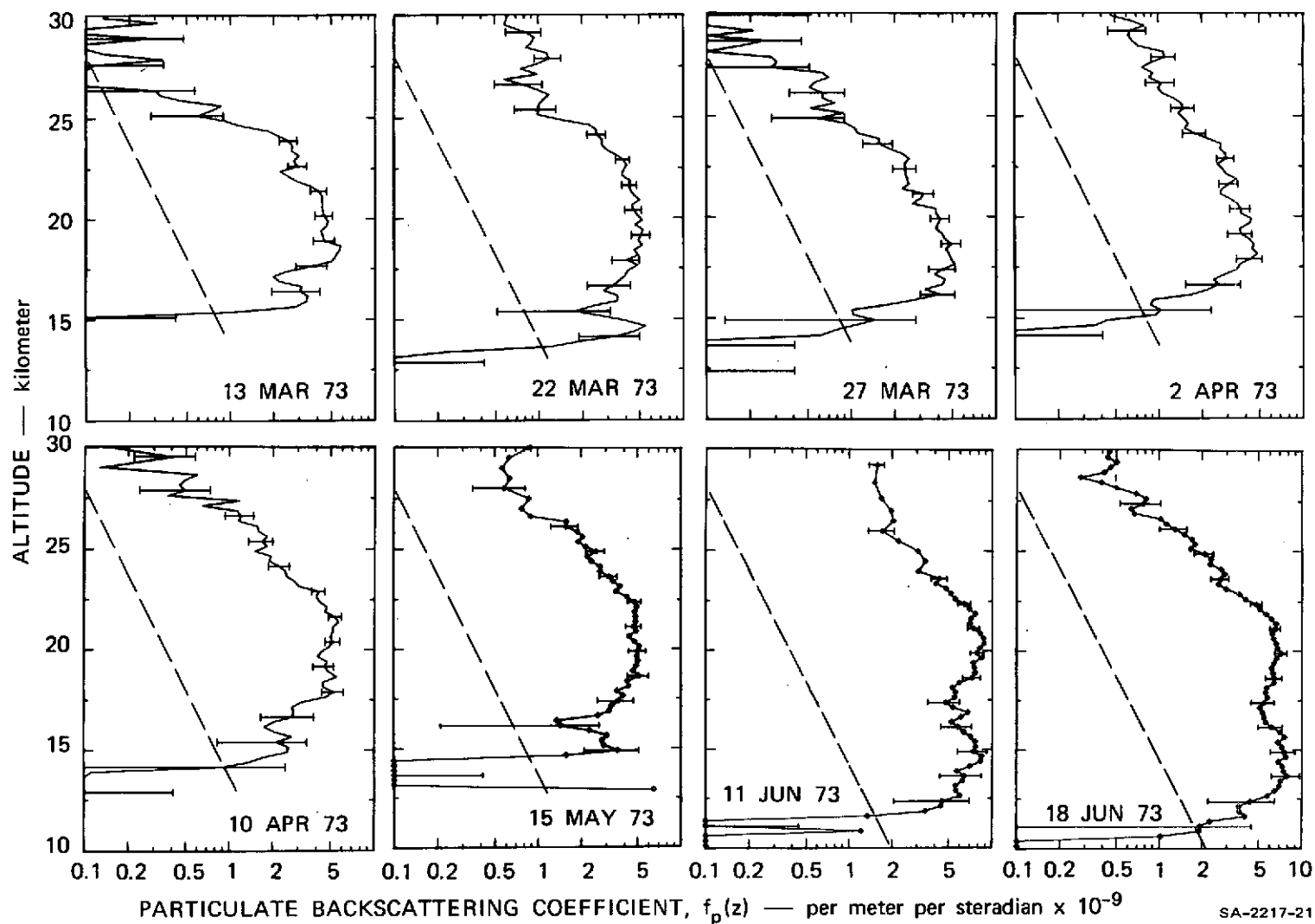


FIGURE 4b TIME SERIES OF PARTICULATE BACKSCATTERING COEFFICIENT AS A FUNCTION OF HEIGHT, DERIVED FROM LIDAR BACKSCATTER OBSERVATIONS ( $\lambda = 0.69 \mu\text{m}$ ) MADE AT MENLO PARK, CALIFORNIA (Continued)

Profiles are computed using Oakland radiosonde sounding for molecular densities, and assuming Rayleigh and ozone extinction as given by Elterman (1968), with no particulate extinction. Error bars are  $\pm 1\sigma$  (shown at every fifth data point). Dashed line is drawn at a constant mixing ratio of 1% of the molecular backscattering coefficient.

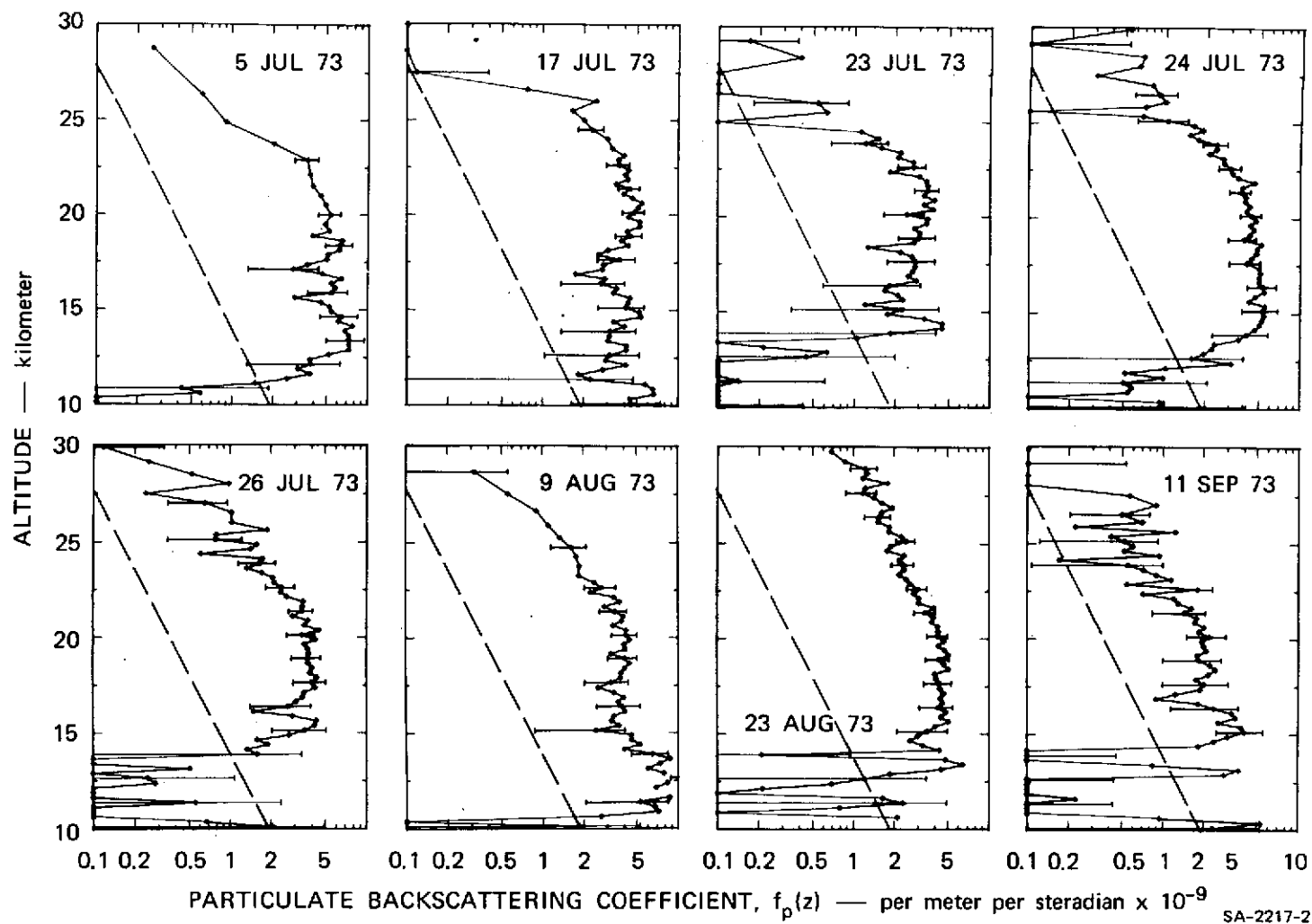
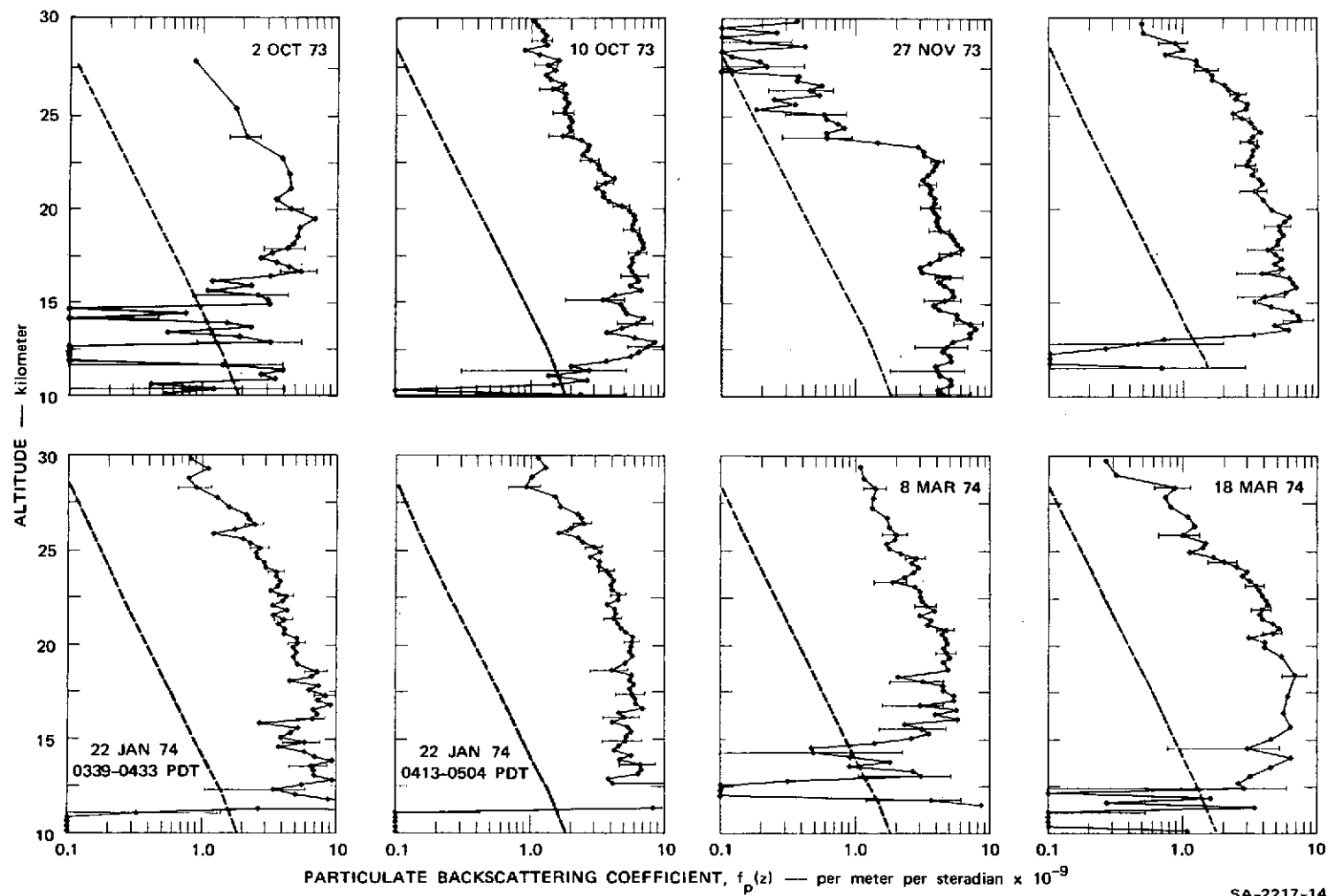


FIGURE 4c TIME SERIES OF PARTICULATE BACKSCATTERING COEFFICIENT AS A FUNCTION OF HEIGHT, DERIVED FROM LIDAR BACKSCATTER OBSERVATIONS ( $\lambda = 0.69 \mu\text{m}$ ) MADE AT MENLO PARK, CALIFORNIA (Continued)

Profiles are computed using Oakland radiosonde sounding for molecular densities, and assuming Rayleigh and ozone extinction as given by Elterman (1968), with no particulate extinction. Error bars are  $\pm 1\sigma$  (shown at every fifth data point). Dashed line is drawn at a constant mixing ratio of 1% of the molecular backscattering coefficient.



SA-2217-14

FIGURE 4d TIME SERIES OF PARTICULATE BACKSCATTERING COEFFICIENT AS A FUNCTION OF HEIGHT, DERIVED FROM LIDAR BACKSCATTER OBSERVATIONS ( $\lambda = 0.69 \mu\text{m}$ ) MADE AT MENLO PARK, CALIFORNIA (Concluded)

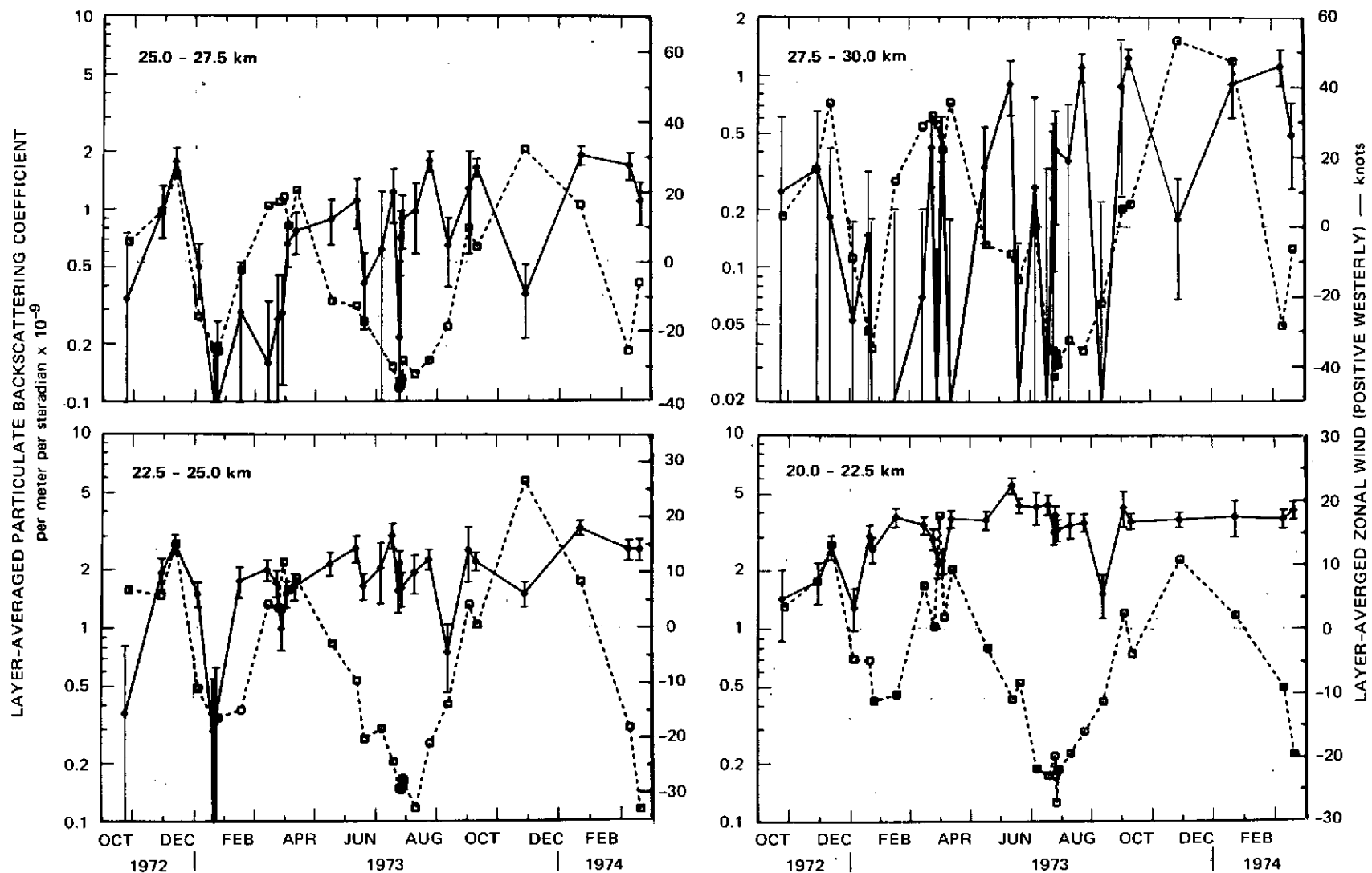
Profiles are computed using Oakland radiosonde sounding for molecular densities, and assuming Rayleigh and ozone extinction as given by Elterman (1968), with no particulate extinction. Error bars are  $\pm 1\sigma$  (shown at every fifth data point). Dashed line is drawn at a constant mixing ratio of 1% of the molecular backscattering coefficient.

1973, Fernald, et al., 1973). The relationship of the current series of measurements to previous measurements made by a variety of techniques is discussed more fully in Section 5.

As can be seen in Figs. 3 and 4, the variability in particulate backscattering is much greater above and below the main Junge layer than within it. In particular, the region between the major peak and 30 km is frequently seen to change from a clean condition ( $R \approx 1$ ) to one where the scattering ratio is nearly as large as in the major peak. At times, in fact, the backscattering mixing ratio,  $R(z)-1$ , appears to be constant above the major peak, and this can also be seen in Fig. 4 by comparing the backscattering profiles with the darkened line of constant mixing ratio.

(b) Relation to winds and sudden stratospheric warming

To facilitate analysis of the time variability of particulate backscattering in various altitude regions, Fig. 5 shows time series of the particulate backscattering coefficient  $f_p(z)$  vertically averaged over four individual layers of 2.5-km thickness. Also shown are values of the layer-averaged zonal component of the local wind (obtained by rawinsondes launched at Point Mugu, California) to permit inspection for any clear correspondence between zonal transport and particulate



SA-2217-24

FIGURE 5 TIME VARIABILITY OF LAYER-AVERAGED PARTICULATE BACKSCATTERING COEFFICIENT (SOLID LINE) AND ZONAL WIND (DASHED LINE) FOR FOUR ALTITUDE REGIONS

content.\* In the 20.0 to 22.5-km layer, which always includes at least part of the major peak, no such obvious correspondence is seen. In general, no clear correspondence is evident in any of the other layers either, with the exception of the period between November 1972 and March 1973 when an apparent correspondence is rather obvious in the 22.5 to 25.0 and 25.0 to 27.5-km layers. Specifically, the sudden decrease in the particulate backscattering coefficient in January 1973 was accompanied by a reversal of wind direction from westerly to easterly. Subsequently, the backscattering coefficient returned to its previous value, and this return was accompanied by a return of the winds to westerly. Similar behavior is suggested in the 27.5 to 30.0-km layer, but the larger relative errors in measured particulate backscattering coefficient make the comparison inconclusive.

This interesting coincidence between wind and particulate behavior occurred at the time of a sudden stratospheric warming (Quiroz 1973). The reason for the apparent correspondence is not understood at the present time. A possible reason is simply the change in direction of advection. However, it should be noted that a similar reduction in particulate content did not occur at the time of the springtime wind reversal, and thus possible differences in sources of winter and

---

\* In this report and in all previous reports, comparisons shown between lidar data and stratospheric wind data are based on analyses performed under SRI-sponsored research. The comparisons are illustrated and described to aid the interpretation of the lidar observations.

summer easterly flows should be considered, or, alternatively, still other mechanisms. A subsidence of cleaner air from above is a possible mechanism that bears further consideration. Alternatively, temperature effects on particle sublimation or evaporation, or on photochemical reaction processes, may be significant factors. The present lack of understanding of the chemistry and thermodynamics of stratospheric aerosol formation and removal makes these possibilities difficult to assess (see also Section 5), but a more careful inspection of this incident, using local temperature and radiance data, is probably warranted. (Note that the comparison data shown in Fig. 5 are limited in space and time, because the Point Mugu wind data were obtained more than 320 km SSE of the lidar site, and during daylight, while the lidar data were collected at night.) The lack of any pronounced effect in the 20.0 to 22.5-km layer may be due to a weakening of the sudden warming with decreasing altitude, or may be associated with the more persistent spatial and temporal quality of the major Junge layer.

Two qualifications of the data shown in Fig. 5 should be appreciated at this point. First of all, lines drawn between data points are drawn only to aid the eye, and not to imply that backscattering coefficients (or winds) necessarily fell on the lines at times between the observation dates. This is especially true after November 1973, when observations were scheduled less frequently to permit more concentration on comparative experiments [see also Section 4(e)].

The second reservation concerns the overall increasing trend in the plotted particulate backscattering coefficients in the 20.0 to 22.5-km layer between October 1972 and June 1973. During this period, the lower bound of the analyzed lidar profiles was gradually being extended downward, from approximately 20 km to 10 km or lower (see Figs. 3 and 4). Thus, generally speaking, the earlier the observation date, the greater was the probability of a significant amount of particulate material actually being present at the "clean" level assumed for normalization of the scattering ratios. As discussed in Section 3, when the matching method of analysis is employed, the presence of particulate material at the assumed "clean" level leads to an underestimate of particulate backscattering at all levels. Thus it is likely that the apparent increasing trend in  $\bar{f}_p$  (20.0 to 22.5 km) in the early data is an artifact of the analysis, rather than an actual stratospheric occurrence. However, this reservation regarding the October 1972 - June 1973 trend does not invalidate the above discussion regarding short-term changes in  $\bar{f}_p$  near the time of the sudden stratospheric warming. Specifically, the lidar profile obtained on January 1973, at the time of minimum  $\bar{f}_p$  (22.5 to 27.5 km), was exceptional in extending down to 13 km, and thus is more likely than the surrounding observations to have included an actual clean layer. In addition, the shape of the scattering ratio profiles on 19 and 22 January 1973 differs significantly from that of most other profiles, with the

peak being lower in altitude and narrower. These shape features are independent of the amount of particulate material at the assumed clean level.

### (c) Particulate Optical Depths

The profiles of particulate backscattering coefficient  $f_p(z)$  shown in Fig. 4 can be converted to profiles of particulate extinction coefficient  $\beta_p(z)$  by using the relation

$$\beta_p(z) = \frac{4\pi}{P(\pi)} f_p(z), \quad (7)$$

where  $P(\pi)/4\pi$  is the backscattering phase function (per steradian) of the polydispersion of aerosol particles at altitude  $z$ . Without measurements of  $P(\pi)$  for actual stratospheric aerosols,  $P(\pi)$  may be computed by using an optical model that is consistent with current experimental measurements of particle size distribution, shape, and refractive index. To indicate the range of results that is possible for a number of selected aerosol characteristics, Table 3 lists values of various light-scattering parameters that were computed using Mie scattering theory (which is valid provided that the particles are homogeneous spheres). The values of  $P(\pi)/4\pi$  listed in Table 3 vary by about a factor of five (0.011 to 0.049), but it must be emphasized that only a subset of the listed particle size distributions and refractive indices may be consistent with current experimental data on particle size, composition, and the like.

Table 3

 LIGHT-SCATTERING AND OTHER PROPERTIES COMPUTED FOR SELECTED  
 AEROSOL SIZE DISTRIBUTIONS AND REFRACTIVE INDICES

Size Distribution	N (cm <sup>-3</sup> )	N <sub>R</sub> /N		N <sub>15</sub> /N <sub>25</sub>	$\bar{V}$ (cm <sup>3</sup> × 10 <sup>-14</sup> )	Refractive Index	$\hat{f}_p$ (m <sup>-1</sup> cm <sup>3</sup> × 10 <sup>-7</sup> )	P(π)/4π	$\hat{f}_p$ (m <sup>-1</sup> sr <sup>-1</sup> cm <sup>3</sup> × 10 <sup>-9</sup> )	$\rho$ (g cm <sup>-3</sup> )	$\bar{m}$ (g × 10 <sup>-14</sup> )	$\hat{f}_p$ (m <sup>-1</sup> sr <sup>-1</sup> g <sup>-1</sup> cm <sup>3</sup> × 10 <sup>4</sup> )
		R = 0.15 μm	R = 0.25 μm									
Deirmendjian Haze II	100	0.423	0.125	3.38	3.14	1.33 <sup>a</sup> 1.40 <sup>b</sup> 1.41 1.42 1.45 <sup>b</sup> 1.54 <sup>a</sup>	0.988 1.36 1.41 <sup>d</sup> 1.47 <sup>d</sup> 1.63 2.07	0.01095 0.01282 0.0131 <sup>d</sup> 0.0134 <sup>d</sup> 0.01431 0.01847	1.08 1.75 1.86 <sup>d</sup> 1.97 <sup>d</sup> 2.33 3.81	1.5	4.73	2.29 3.69 3.94 <sup>d</sup> 4.17 <sup>d</sup> 4.92 8.09
Deirmendjian Haze I.	100	0.474	0.236	2.01	11.7	1.42 1.33 <sup>a</sup> 1.40 <sup>b</sup> 1.41 1.45 <sup>b</sup>	1.47 3.95 4.47 4.52 <sup>d</sup> 4.73	0.0134 <sup>d</sup> 0.01002 0.01605 0.01777 <sup>d</sup> 0.02465	1.97 <sup>d</sup> 3.96 7.17 8.03 <sup>d</sup> 11.66	1.63 1.5	5.12 17.55	3.84 2.26 4.09 4.59 <sup>d</sup> 6.64
"Junge"												
r <sub>1</sub> (μm)	r <sub>2</sub> (μm)											
0.04	10.0	2.5		3.59	1.98	1.5 <sup>c</sup>	0.290	0.049	1.39	1.5		4.68
		3.0		4.63	0.444	1.5 <sup>c</sup>	0.101	0.039	0.390	1.5		5.86
		3.5		5.98	0.176	1.5 <sup>c</sup>	0.407	0.034	0.140	1.5		5.30
		4.0		7.72	0.107	1.5 <sup>c</sup>	0.0185	0.035	0.652	1.5		4.06
0.08	10.0	2.5		3.59	10.9	1.5 <sup>c</sup>	1.63	0.049	7.80	1.5		4.77
		3.0		4.63	3.10	1.5 <sup>c</sup>	0.797	0.038	3.02	1.5		6.49
		3.5		5.98	1.37	1.5 <sup>c</sup>	0.448	0.032	1.45	1.5		7.06
		4.0		7.72	0.851	1.5 <sup>c</sup>	0.279	0.031	0.859	1.5		5.67
0.04	3.0	2.5		3.59	1.03	1.5 <sup>c</sup>	0.262	0.045	1.19	1.5		7.70
		3.0		4.63	0.347	1.5 <sup>c</sup>	0.0977	0.035	0.369	1.5		7.07
		3.5		5.98	0.166	1.5 <sup>c</sup>	0.0404	0.034	0.137	1.5		5.50
		4.0		7.72	0.106	1.5 <sup>c</sup>	0.0184	0.035	0.0648	1.5		4.08
0.08	3.0	2.5		3.59	5.50	1.5 <sup>c</sup>	1.47	0.045	6.66	1.5		8.07
		3.0		4.63	2.32	1.5 <sup>c</sup>	0.772	0.037	2.84	1.5		8.16
		3.5		5.98	1.26	1.5 <sup>c</sup>	0.445	0.032	1.42	1.5		7.51
		4.0		7.72	0.837	1.5 <sup>c</sup>	0.278	0.030	0.855	1.5		6.81

 Notes:  $n(r) dr$  = number of particles per unit volume with radii between  $r$  and  $r + dr$ .

 $N_R = \int_R^\infty n(r) dr$  = number of particles, with radii larger than  $R$ .

 $\bar{V} = 4\pi/3 \int_0^\infty r^3 n(r) dr$  = mean volume per particle.

 $N = N_0$  = number of particles of all sizes.  $\bar{m} = \bar{m} =$  mean mass per particle.

For other symbol definitions see Section 4 of text.

<sup>a</sup> Mie scattering results taken from Deirmendjian (1969) [ $\lambda = 700$  nm].

<sup>b</sup> Mie scattering results computed in this laboratory [ $\lambda = 700$  nm].

<sup>c</sup> Mie scattering results taken from McCormick, et al. (1968) [ $\lambda = 694.3$  nm].

<sup>d</sup> Obtained by interpolation of values for 1.40, 1.45 refractive index.

A model value from Table 3 that we adopt for the present discussion is

$$P(\pi)/4\pi = 0.0132, \quad (8)$$

which is obtained for the purely real refractive index  $m = 1.42$  and the Deirmedjian (1969) haze H size distribution. This refractive index corresponds to a particle composition of 75 percent sulfuric acid and 25 percent water (by mass). This particle composition and this size distribution are consistent with a number of recent experimental results, as is discussed more fully in Section 4(e). By using Eqs. (7) and (8), we converted the particulate backscattering coefficient profiles of Fig. 4 to profiles of particulate extinction coefficient  $\beta_p$ . From these profiles, values of the integrated particulate optical thickness, given by

$$\Delta\tau_p(z_2, z_3) = \int_{z_2}^{z_3} \beta_p(z) dz, \quad (9)$$

were then computed for a number of layers  $(z_2, z_3)$ . Selected results are shown in Fig. 6.

For the upper layers (i.e., lower curves) shown in Fig. 6, the particulate optical thickness shows quite a bit of time variability, including the sudden decline during the January 1973 stratospheric warming, which was discussed in Section 4(b). Values integrated upward through lower layers, including the major peak, show much less variability, especially when the probable artificiality of the upward trend between November 1972 and June 1973 is considered [see Section 4(b)]. On the whole, it is difficult to see any generally increasing or decreasing

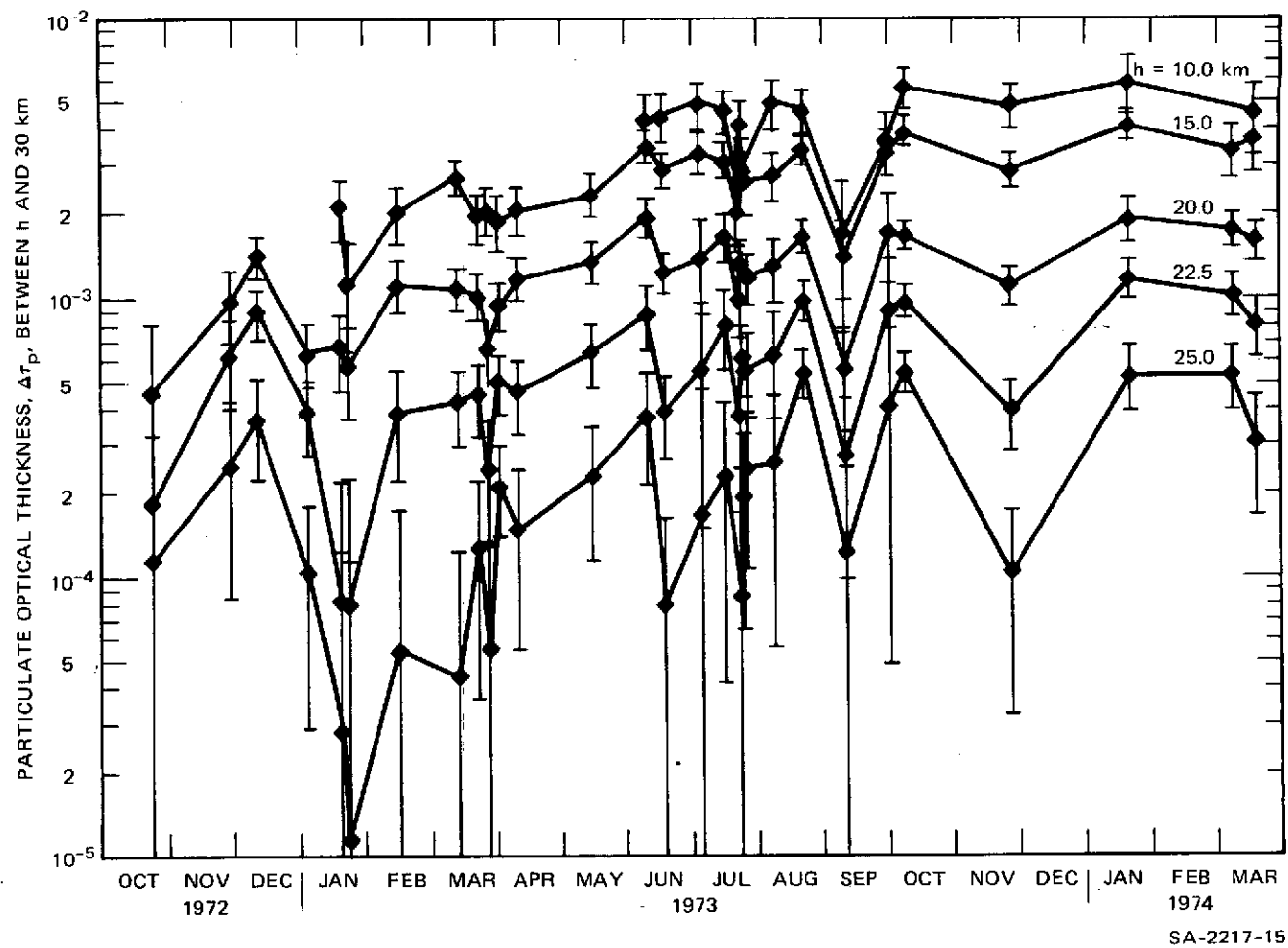


FIGURE 6 TIME VARIABILITY OF PARTICULATE OPTICAL THICKNESS FOR SEVERAL ALTITUDE REGIONS

Values are derived from lidar-measured particulate backscattering coefficients by assuming the backscattering phase function  $P(\pi)/4\pi = 0.0134$  (Deirmendjian haze H size distribution, spherical particles,  $\lambda = 0.7 \mu\text{m}$ , refractive index  $n = 1.42$ ). For the 10–30 km layer, dates have been omitted if cirrus was present.

trend in the particulate optical thickness data. Similarly, as noted by Reiter (1971) in summarizing previous data, there does not appear to be any regular seasonal pattern to the time variability.

For the phase function of Eq. (8), our derived values of particulate optical depth in the 12- to 25-km layer fall in the range

$$\Delta\tau_p(12, 25) = 1.6 \text{ to } 4 \times 10^{-3}. \quad (\lambda = 693 \text{ nm, 1973-74 lidar})$$

Assuming a  $\lambda^{-1}$  wavelength-dependence [cf. Elterman, 1968, Elterman et al., 1973; Deirmendjian, 1972; and Section 4(d)], these may be converted to

$$\Delta\tau_p(12, 25) = 2 \text{ to } 5 \times 10^{-3}. \quad (\lambda = 550 \text{ nm, 1973-74 lidar})$$

For comparison, Elterman's model (1968), based on searchlight measurements made in 1964 and 1965 and the phase function of Reeger and Seidentopf (1946) gives

$$\Delta\tau_p(12, 25) = 2.4 \times 10^{-2}. \quad (\lambda = 550 \text{ nm, 1964-5 searchlight})$$

More recent searchlight measurements, made in late 1970 (Elterman et al., 1973), give

$$\Delta\tau_p(12, 25) = 2.0 \times 10^{-2}. \quad (\lambda = 550 \text{ nm, 1970 searchlight})$$

Thus our present determination of stratospheric particulate optical thickness is smaller by a factor of 5 to 12 than the 1964-65 searchlight determination, and smaller by a factor of 4 to 10 than the 1970 searchlight determination. The implied temporal decline in stratospheric

turbidity, and other possible differences between the lidar and search-light measurements, are discussed in Section 5.

It is emphasized that the optical thicknesses shown in Fig. 6 are based on the assumed backscatter phase function given in Eq. (8). Choice of a different phase function [e.g., from Table 3, or the value  $P(\pi)/4\pi = 0.0143$  of Reeger and Seidentopf (1946)] would change all of the derived values according to Eq. (7). For example, if the stratospheric particles are shown to be predominantly irregular plates, rather than spheres, then  $P(\pi)$  should probably be substantially reduced, (Holland and Gagne 1970), thus substantially increasing all inferred optical thicknesses. A similar result would apply if the particles are shown to be absorptive at the lidar wavelength (i.e., have a nonzero imaginary refractive index). Nevertheless, any phase function considered for use should be consistent with applicable recent measurements of the optical, chemical, and physical properties of the stratospheric aerosol. This requirement greatly restricts the choice of possible backscatter phase functions, and is discussed more fully in Sections 4(e) and 5.

The above lidar-derived values of  $\Delta\tau_p$  give a two-way particulate optical transmission at the ruby wavelength of

$$q_p^2(30 \text{ km}) = \exp \left[ -2\Delta\tau_p(10, 30) \right] = 0.997 \text{ to } 0.990,$$

assuming a lower profile-analysis bound of 10 km. The values will vary by several tenths of a percent depending on the date of the lidar observation and the assumed (realistic) value of  $P(\pi)$ . However, for the

present range of observed lidar scattering ratios,  $q_p^2(z)$  will always differ from unity by less than our observational accuracy (for scattering ratios) of approximately two percent. Therefore, in deriving scattering ratio profiles (cf., Section 3), we have chosen to adopt a model of unit particulate transmission (i.e.,  $q_p^2(z) \equiv 1$ ) rather than adopt some other value (e.g., 0.992) that implies an accuracy in determining stratospheric particulate extinction that cannot presently be justified. For purposes of comparison, the Elterman (1968) model value for  $q_p^2(30 \text{ km})$  with a lower analysis bound of 10 km is 0.947. As can be seen from Eqs. (3) and (4), use of this value would change some of our present results by more than two standard errors. An example of such a change has been given by Russell et al., (1973a).

In computing the Rayleigh scattering and ozone absorption components of the two-way transmission  $q^2(z)$ , we have used the model profiles given by Elterman (1968). As shown by Russell et al., (1973a), extremely large changes in atmospheric density and ozone concentration are required to introduce significant error into the resulting value of  $q^2(z)$ . However, because of the uncertainty in  $P(\pi)$  and the variability in stratospheric particulate content, we have adopted a value of 1 percent as the estimated uncertainty in  $q_p^2(z)$ , and thus also in  $q^2(z)$ .

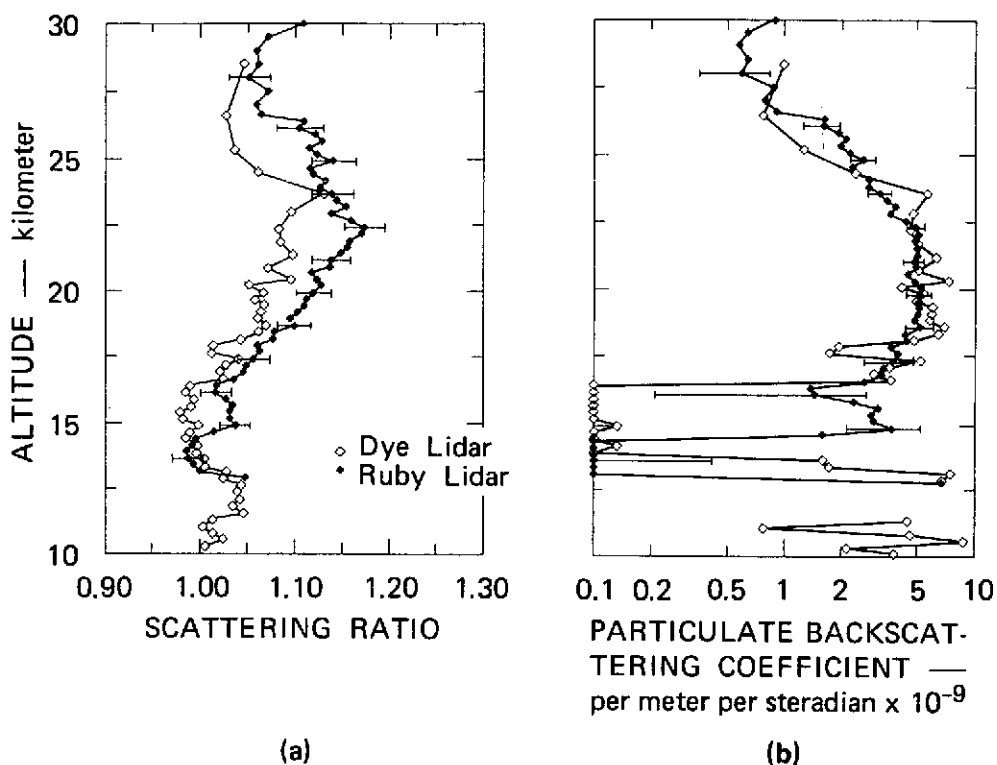
#### (d) Sequential ruby and dye lidar observations

On the night of 15-16 May 1973, observations were made between 2203 and 2258 PDT using the ruby laser ( $\lambda = 694.3 \text{ nm}$ ) transmitter of the lidar system and shortly thereafter, between 0130 and 0419 PDT, using the

dye laser ( $\lambda = 589$  nm) transmitter. (Add seven hours to PDT to obtain GMT.) The results are shown in Fig. 7. As can be seen from Fig. 7(a), the observations at both wavelengths reveal a scattering ratio profile of similar shape; however, the values at the shorter dye wavelength fall consistently below those at the ruby wavelength. This is in accord with the  $\lambda^{-4}$  dependence of molecular (Rayleigh) backscattering and the expected weaker  $\lambda^{-\alpha}$  dependence of particulate backscattering [typically observed values are  $\alpha = 0$  to  $2$ ; for example Elterman's (1968) model uses  $\alpha \approx 0.9$ ]. Thus, at the shorter dye wavelength, molecular scattering may be expected to be relatively more important than particulate scattering when compared with the relative amounts of scattering at the longer ruby wavelength. This expected behavior is indeed observed in Fig. 7(a) and confirms the fact that the enhanced backscattering in the 18- to 25-km region does not result from an anomalously dense molecular layer (which would give scattering ratios independent of wavelength) but must be of particulate origin. In addition, the fact that the scattering ratio profiles have the same shape tends to validate the radiosonde density profile used in the computation of the scattering ratios.

The wavelength-dependence of the particulate backscattering coefficient  $f_p$  may be simply related to the particle size distribution  $n(r)$  ( $r$  is particle radius), provided that the size distribution is of the form

$$n(r) = K_1 r^{-(\nu + 1)} \quad (10)$$



SA-2217-23

FIGURE 7 COMPARISON OF LIDAR PROFILES MEASURED WITH RUBY TRANSMITTER ( $\lambda = 0.6943 \mu\text{m}$ , 2203-2258 PDT) AND DYE TRANSMITTER ( $\lambda = 0.5890 \mu\text{m}$ , 0130-0419 PDT) AT MENLO PARK, CALIFORNIA, ON 15-16 MAY 1973

(a) Scattering ratio; (b) Particulate backscattering coefficient

throughout the optically significant size range. If this is the case, it can easily be shown [see e.g., Junge 1963, p. 142] that

$$f_p = K_2 \lambda^{-\alpha} \quad (11)$$

and

$$\alpha = \nu - 2 \quad (12)$$

In these equations,  $K_1$  and  $K_2$  are constants proportional to the particle number concentration, and  $\nu$  is a single parameter giving the dependence of particle number on radius. As can be seen from Fig. 7(b), the

15 May 1973 observation is inadequate to make an accurate determination of the wavelength exponent  $\alpha$  because the ruby and dye values do not generally differ from each other by more than the uncertainty of the respective measurements. Within that uncertainty, however, the wavelength-dependence of  $f_A$  shown in Fig. 7(b) is consistent with values of  $\alpha$  in the approximate range of -0.5 to 1.0. These correspond to size distribution exponent values of  $\nu = 1.5$  to 3, which are consistent with values observed experimentally [Junge et al., 1961a,b ( $\nu \approx 1.5$  to 3)], and also with values derived from two-threshold particle counters [Hofmann et al., 1973; Russell et al., 1973b ( $\nu = 2.7 \pm 0.5$ )], and values expected on the basis of theoretical considerations [Friedlander 1961 ( $\nu = 1$  to 3)]. These results are encouraging, but primarily they tend to emphasize the need for somewhat higher precision in the acquisition and analysis of stratospheric lidar data if useful wavelength-dependencies and size distribution information are to be extracted. The development of higher-power dye lasers makes this greater precision a reasonable possibility. A higher-precision system should also have a dual-transmitter configuration to permit dye and ruby profiles to be acquired in rapid and alternating sequence, thus minimizing ambiguities due to time variations in stratospheric aerosol structure.

#### (e) Comparative lidar/direct-sampling experiments

In the present study, three aircraft sampling experiments were conducted over the lidar site at times coincident with, or very close to,

lidar observations. The particle concentration data obtained by such aircraft sampling provided a test of the validity of particulate backscattering coefficients derived from lidar data by using the matching method of analysis, and also provided information on particle size distribution, shape, and chemical composition for use in converting lidar backscattering data to other optical and physical parameters. A previous lidar/direct sampling experiment, the Laramie Comparative Experiment, has been described by Dynatrend (1973), Fernald et al., (1973), and Melfi et al. (1973).

(1) WB-57F Overflight. On 26 July 1973 a WB-57F aircraft, specially instrumented for the Climatic Impact Assessment Program, made in situ measurements at an altitude of  $61,000 \pm 500$  ft ( $18.7 \pm 0.15$  km) MSL over the SRI lidar site. (The stated uncertainties result from the response characteristics of autopilot operation and altitude-measuring instrumentation on the aircraft.) A sample of ambient particulate material was collected using a wing-pod filter sampler provided by William A. Sedlacek of Los Alamos Scientific Laboratory, University of California, Los Alamos, New Mexico. This sample was subsequently returned to the National Center for Atmospheric Research, Boulder, Colorado, where it was analyzed for chemical composition and mass by Bruce Grandrud and Alan Lazrus.

The results of the laboratory analysis (Sedlacek, private communication 1973) are summarized in Table 4. No silicates or other materials

Table 4

## COMPARISON OF LIDAR OBSERVATIONS WITH WB-57F AIRCRAFT MASS SAMPLING MEASUREMENT

Method of Observation	1	2	Particle Characteristics					Ambient Aerosol Characteristics		
	1973 Date	Time (PST)	3	4	5	6	7	8	9	10
			Chemical Composition	Density (g cm <sup>-3</sup> )	Refractive Index	Shape	Assumed Size Distribution	Particulate Back-scattering Coefficient $f_p$ (m <sup>-1</sup> sr <sup>-1</sup> × 10 <sup>-9</sup> )	Number Concentration, N (cm <sup>-3</sup> ) <sup>a</sup>	Mass Concentration, M (g cm <sup>-3</sup> × 10 <sup>-14</sup> )
WB-57F Aircraft (filter sample, 18.7 ± 0.15 km)	26 July	0819-0906	Sulfuric acid and water solution (5.8 × 10 <sup>-14</sup> g cm <sup>-3</sup> SO <sub>4</sub> <sup>2-</sup> ambient) <sup>a</sup>	1.63 <sup>b</sup>	1.42 <sup>c</sup>	Amorphous (frozen) or spherical (supercooled liquid) droplets <sup>d</sup>	Deirmendjian Haze H		1.5 ± 0.3 <sup>e</sup>	7.9 ± 1.5 <sup>b</sup>
Lidar (18.5 - 18.8 km, $\lambda = 0.69 \mu\text{m}$ )	23 July	2030-2300						2.9 ± 0.9 <sup>g</sup>	1.5 ± 0.5 <sup>h</sup>	7.5 ± 2.3 <sup>i</sup>
	24 July	2100-2342						4.8 ± 0.9 <sup>g</sup>	2.4 ± 0.5 <sup>h</sup>	12.5 ± 2.3 <sup>i</sup>
	26 July	2210-0030						3.7 ± 0.9 <sup>g</sup>	1.9 ± 0.5 <sup>h</sup>	9.6 ± 2.3 <sup>i</sup>

\* Note that N is the total number of particles (per unit volume) of all sizes. A photoelectric particle counter would measure only the fraction  $N_R/N$  of this total (see Table 3).

<sup>a</sup> Aircraft measurement.

<sup>b</sup> Best estimate from aircraft measurement of chemical composition and results of Rosen (1971), and Toon and Pollack (1973).

<sup>c</sup> Inferred from aircraft measurement (Columns 3 and 4) using standard tabulation at 18.3°C.

<sup>d</sup> Inferred from aircraft measurement (Columns 3 and 4, plus ambient temperature [-61°C], plus room temperature analysis showing no solid particles larger than instrument resolution of 0.2  $\mu\text{m}$ ).

<sup>e</sup> Computed from aircraft measurement (Column 10) using value of  $\bar{m}$  (see Table 3) consistent with Columns 4, 6 and 7.

<sup>f</sup> Computed from aircraft measurement (Column 3) using specific gravity from Column 4.

<sup>g</sup> Lidar measurement.

<sup>h</sup> Computed from lidar measurement (Column 8) using value of  $\hat{f}_p$  (see Table 3) consistent with Columns 3, 5 to 7.

<sup>i</sup> Computed from lidar measurement (Column 8) using value of  $\hat{f}_p$  (see Table 3) consistent with Columns 3 to 7.

that are solid at room temperature were detected by a scanning electron microscope having a resolution of 0.2  $\mu\text{m}$ . Chemical analysis revealed a particle composition that was essentially a solution of sulfuric acid and water, with negligible amounts of trace elements present. The ambient mass concentration of sulfate ion ( $\text{SO}_4^{=}$ ) at the flight altitude was determined to be  $(5.8 \pm 1.1) \times 10^{-14} \text{ g cm}^{-3}$ , or  $(5.9 \pm 1.1) \times 10^{-14} \text{ g cm}^{-3}$  of pure sulfuric acid. The stated uncertainties ( $\pm 1\sigma$ ) result from an estimated 10 percent probable error in sampled air volume and an estimated 15 percent probable error in measured sulfate mass.

The acid/water mass mixing ratio of the solution droplets in the stratosphere is determined by the ambient relative humidity, data for which were not available in this experiment. Toon and Pollack (1973) have recently shown that values of the acid mass fraction between approximately 40 and 80 percent are possible, and that 75 percent is the most probable value. This latter value is also in agreement with a previous determination by Rosen (1971), based on the measured boiling point of stratospheric particles. We therefore initially adopt an acid/water mass mixing ratio of 75/25 as the best estimate for the aerosol sampled by the WB-57F. This estimate implies a total ambient mass concentration of solution droplets given by

$$M = (1./0.75) \times (5.9 \pm 1.1) \times 10^{-14} \text{ g cm}^{-3} = (7.9 \pm 1.5) \times 10^{-14} \text{ g cm}^{-3} \quad (13)$$

and a solution mass density (specific gravity) of

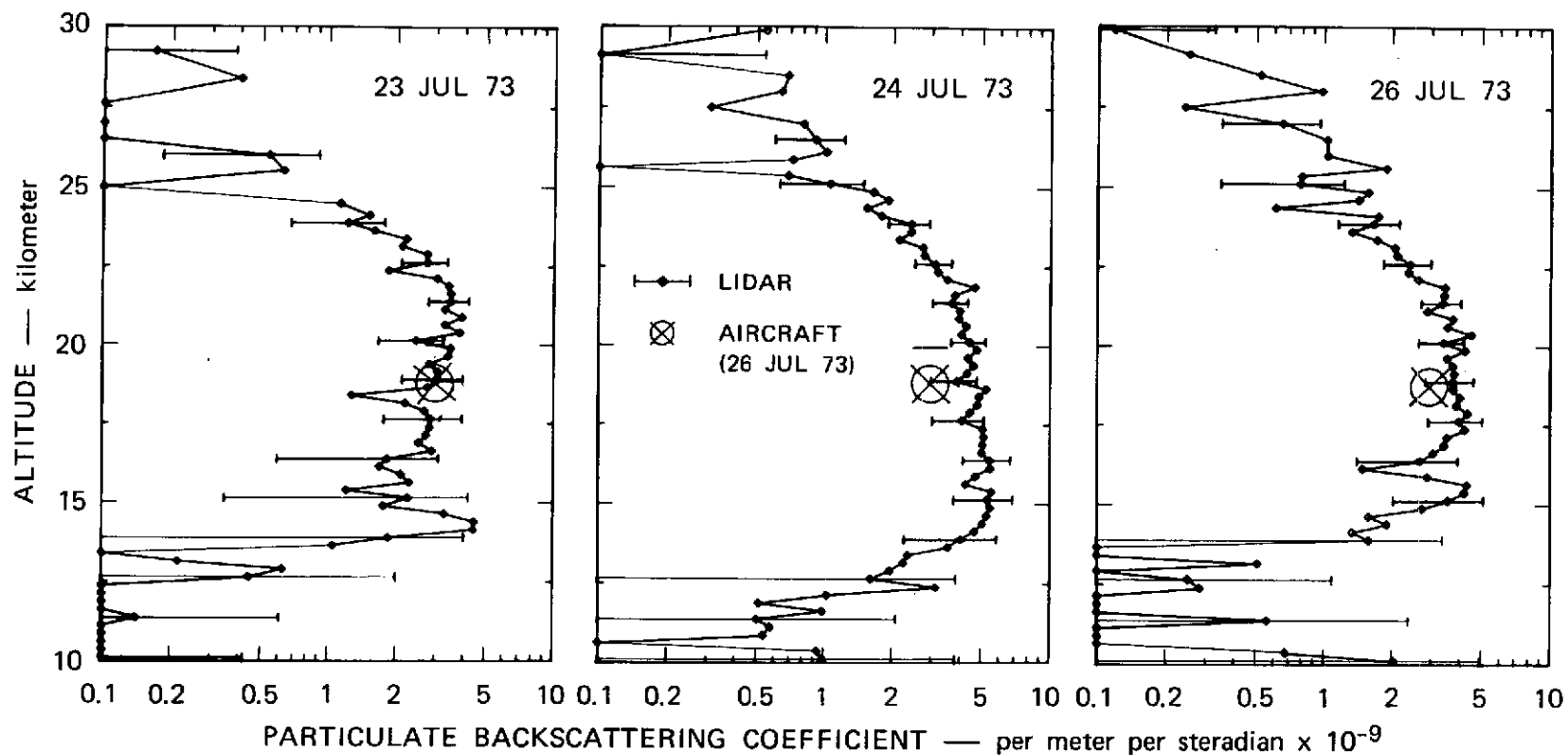
$$\rho = 1.63 \text{ g cm}^{-3} \quad (14)$$

We made lidar observations on the night following the WB-57F over-flight (26 July) and also on two nights shortly before the flight (23 and 24 July). The resulting vertical profiles of particulate backscattering coefficient  $f_p(z)$  are shown in Fig. 8. For purposes of comparison, we have assumed that the aircraft filter sample represents an average over the probable boundaries of the flight altitude ( $18.7 \pm 0.15$  km MSL). Values of  $f_p(z)$  averaged over this interval ( $z = 18.55$  to  $18.85$  km) are listed in Table 4. [The sources of the stated uncertainties in  $f_p$  are given in Section 3(b).]

To convert the values of  $f_p(z = 18.55 \text{ to } 18.85 \text{ km})$  to unambiguous values of particulate mass concentration, it is necessary to know the refractive index, shape, and size distribution of the particulates. The first two of these factors may be inferred from the laboratory analysis and estimated solution acidity. Standard Tabulations (see, for example, Table 5) show that for all visible wavelengths the specific gravity given by Eq. (14) corresponds to a room-temperature refractive index of

$$m = 1.42 \quad (15)$$

Lacking any definite knowledge of the temperature-dependence of the refractive index, we adopt the value given by Eq. (15) as the best estimate of the particulate refractive index at ambient stratospheric temperatures ( $T \approx -60^\circ\text{C}$ ). The use of a purely real refractive index is supported by



SA-2217-5R

FIGURE 8 COMPARISON OF LIDAR-MEASURED PARTICULATE BACKSCATTERING COEFFICIENTS WITH COMPUTED VALUE BASED ON AIRCRAFT MASS SAMPLER MEASUREMENT

The computation assumes an aerosol mass density of  $1.63 \text{ g cm}^{-3}$ , the Deirmendjian Haze H size distribution (spherical particles),  $\lambda = 0.7 \text{ } \mu\text{m}$ , and refractive index  $m = 1.42$ . See text for details.

Table 5

REFRACTIVE INDEX OF SULFURIC ACID-WATER  
SOLUTIONS FOR VISIBLE WAVELENGTHS

T (°C)	$\rho$ (g cm <sup>-3</sup> )	$\lambda$ (nm)			
		397	486	589	656
18.3	1.811	1.44883	1.44168	1.43669	1.43444
18.3	1.632	1.43694	1.42967	1.42466	1.42227
18.3	1.221	1.38158	1.37468	1.37009	1.36793
18.3	1.028	1.34938	1.34285	1.33862	1.33663

a recent literature review and experimental study by Neumann (1973), which showed that aqueous sulfuric acid solutions are not absorptive in the wavelength region ( $\lambda \approx 700$  nm) of the ruby lidar.

The effects of low stratospheric temperatures and pressures also pertain to the question of particle shape. If the droplets are in the liquid phase, they may be taken to be spheres, and thus the freezing point of the droplets is an important consideration. As discussed by Toon and Pollack (1973), the freezing curve of Giaque et al., (1960) indicates that the equilibrium state of concentrated sulfuric acid solutions is solid (frozen) at stratospheric temperatures (i.e.,  $< -50^\circ\text{C}$ ). However, it is possible for the droplets to exist as supercooled liquid; therefore Toon and Pollack conclude that there is insufficient experimental evidence at present to determine the droplet phase conclusively. This is especially so since trace amounts of nitric acid may be present

in the sulfuric acid droplets, and this presence would cause a significant lowering of the droplet freezing temperature (Castleman 1974). It should also be noted that the characteristics of particle adherence to wires in recent stratospheric collection experiments suggest that at least an outer coating of the particles is liquid (Ferry, private communication 1974). Moreover, the high viscosity of concentrated sulfuric acid leads to the expectation that even if the particles are solid, they may be amorphous, rather than crystalline, in shape (Sedlacek, private communication 1975). We have therefore adopted a model of spherical particles in evaluating the electromagnetic scattering properties of the particles.

The particle size distribution was not measured on the WB-57F overflight, and we have therefore adopted a model analytical size distribution in our analysis. The model that appears most appropriate is the haze H model of Deirmendjian (1969), for the following reasons: (1) it was constructed by Deirmendjian (1969, 1972) to be representative of the stratospheric aerosol measurements of Junge et al. (1961a,b) and Mossop (1964); (2) it is consistent with the ratios of numbers of particles larger than  $0.3\text{ }\mu\text{m}$  and  $0.5\text{ }\mu\text{m}$  obtained by photoelectric particle counters on numerous balloon flights by Hofmann et al. (1972); and (3) when used with a refractive index between 1.40 and 1.45 it yields a computed backscatter-to-particle-number ratio that agrees with values measured in the Laramie Comparative (lidar/balloon) Experiment (Dynatrend 1973).

These reasons have been demonstrated in more detail by Russell et al. (1973b), who also show that the model distribution haze L does not satisfy any of these criteria.

The particle characteristics given above permit the calculation of a number of parameters that are useful in comparing lidar and direct-sampling measurements. The parameters include:

$\bar{v}$   $\equiv$  mean volume per particle [units:cm<sup>3</sup>],

$\bar{m}$   $\equiv$  mean mass per particle [g],

$\beta_p^A$   $\equiv$  extinction coefficient per particle per unit volume [m<sup>-1</sup> cm<sup>3</sup>],

$f_p^A$   $\equiv$  backscattering coefficient per particle per unit volume [(m-sr)<sup>-1</sup> cm<sup>3</sup>],

$\tilde{f}_p$   $\equiv$  backscattering coefficient per particulate mass per unit volume [(m-sr)<sup>-1</sup> g<sup>-1</sup> cm<sup>3</sup>].

Computed values of these parameters are listed in Table 3 for a number of particle characteristics. For the conditions of the WB-57F overflight, a set of characteristics (i.e., an optical model) which appears appropriate, is a model of spherical particles with refractive index  $m = 1.42$ , specific gravity 1.63 (75 percent sulfuric acid, 25 percent water) and size distribution haze H. By using the corresponding value of  $\tilde{f}_p$  from Table 3 and the relation

$$M = f_p / \tilde{f}_p, \quad (16)$$

we have converted the lidar-measured values of  $f_p$  to the ambient particulate mass concentrations shown in Column 10 of Table 4. Within the

uncertainties of the respective measurements,  $M(\text{filter sample})$  is seen to agree with the value of  $M(\text{lidar})$  measured on 26 July (the night following the overflight) and also that measured on 23 July. The difference between  $M(\text{filter sample})$  and  $M(\text{lidar}, 24 \text{ July})$  is slightly greater than the combined 1 $\sigma$  uncertainties, and could possibly be due to changing stratospheric conditions between the night of 24 July and the morning of 26 July.

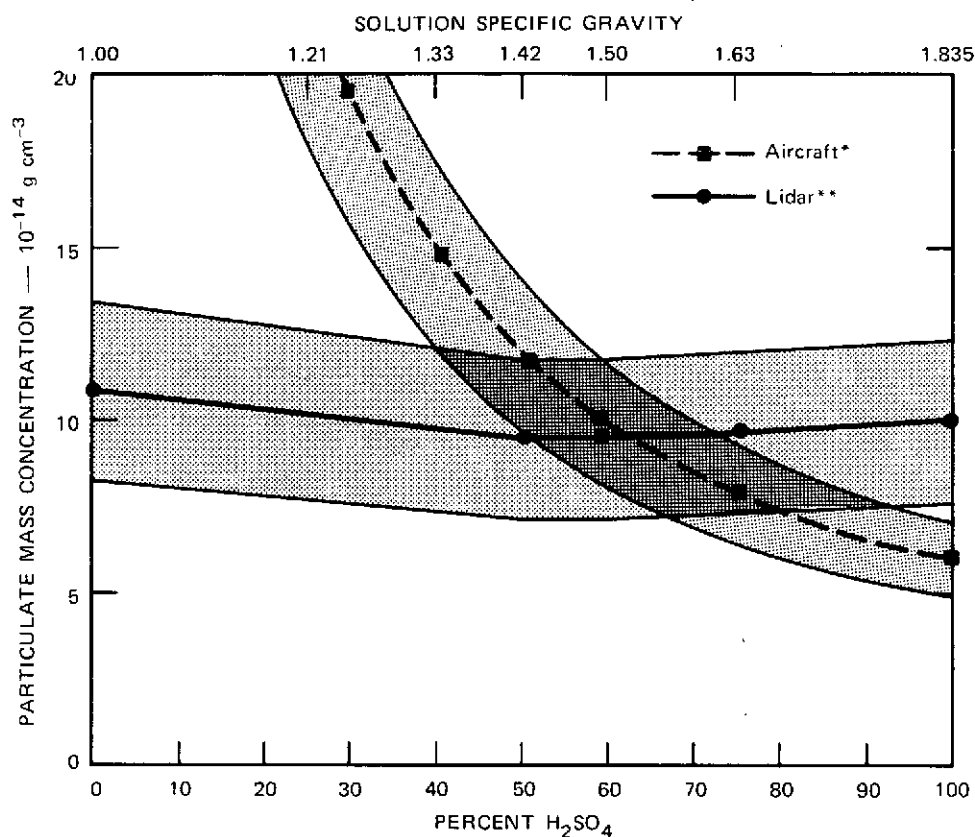
Equation (16) may be rearranged and used to derive a particulate backscattering coefficient  $f_p$  (filter sample) from the aircraft mass measurement. The result thus obtained is plotted in Fig. 8, indicating the relationship between the lidar--measured and aircraft-inferred values.

The agreement shown in Table 4 and Fig. 8 is encouraging, but its sensitivity to some of the assumptions made in adopting the particulate optical model remains to be investigated. From Table 3 it can be seen that values of  $\tilde{f}_p$  [and thus of  $M(\text{lidar})$  and  $f_p$  (filter sample)] are relatively insensitive to changing size distribution. However, for a given specific gravity,  $\tilde{f}_p$  is quite sensitive to assumed refractive index, and for a given refractive index it is of course quite sensitive to assumed specific gravity, as is the value of  $M(\text{filter sample})$ . Both refractive index and specific gravity are determined by the acidity of the droplet solution, which, as noted by Toon and Pollack (1973), could possibly lie between 40 percent and 80 percent, depending on the ambient relative humidity.

Therefore we have repeated the lidar/aircraft mass comparison for a range of assumed acid concentrations. The results are shown in Fig. 9, where the assumed value of  $f_p$  is that measured by the lidar on 26 July at the aircraft flight altitude. The value of  $M(\text{filter sample})$  shows its expected strong dependence on solution acidity. For  $M(\text{lidar})$ , however, the dependence on specific gravity is opposite to that on refractive index, so that the two effects tend to cancel. As a result, for a droplet composition of aqueous sulfuric acid, the inferred value of  $M(\text{lidar})$  is nearly independent of acid concentration. It is seen that  $M(\text{lidar})$  and  $M(\text{filter sample})$  agree within error bars for any assumed acid mass fraction between 40 percent and 94 percent. Moreover for an assumed acidity of 60 percent (a not unreasonable value) the agreement between  $M(\text{lidar}, 26 \text{ July})$  and  $M(\text{filter sample})$  is excellent, and both  $M(\text{lidar}, 23 \text{ July})$  and  $M(\text{lidar}, 24 \text{ July})$  agree with  $M(\text{filter sample})$  within error bars.

This type of agreement lends support to the matching method of lidar data analysis described in Section 3 and used in the present study, especially since the error bars on lidar-inferred quantities do not include any contribution to account for possible particulate content at the assumed clean level.

(ii) Convair 990 Overflight. On 21 January 1974, a NASA Convair 990 made passes over the SRI lidar site at seven altitudes ranging from 3.1 to 12.2 km. The upper three flight altitudes and times are given in Table 6 and shown in Fig. 10. Measurements of ambient particle number



SA-2217-8R

FIGURE 9 DEPENDENCE OF LIDAR- AND AIRCRAFT-INFERRED PARTICULATE MASS CONCENTRATION ON ASSUMED ACID FRACTION OF SULFURIC ACID-WATER SOLUTION

The aircraft curve assumes  $M(\text{H}_2\text{SO}_4) = (5.9 \pm 1.1) \times 10^{-14} \text{ g cm}^{-3}$ .  
 The lidar curve assumes  $f_p = (3.7 \pm 0.9) \times 10^{-9} \text{ m}^{-1} \text{ sr}^{-1}$ ,  $\lambda = 0.7 \mu\text{m}$ ,  
 Deirmendjian haze H size distribution. The shaded areas indicate the  
 estimated uncertainties ( $\pm 1\sigma$ ) in the respective measurements.

density were made by using an Aitken nucleus counter and a Royco particle counter provided by Dan Briehl of NASA Lewis Research Center, Cleveland, Ohio. The results of the Royco particle counter measurements (Briehl, private communication 1974) are shown in Table 6 for the three upper levels. Since the particles measured by the Aitken nucleus counter are too small to be optically significant (i.e., to provide a significant

Table 6

## COMPUTATION OF SCATTERING RATIOS FROM CONVAIR 990 PARTICLE NUMBER DATA

Time, PDT	z (km)	$\Delta N^*$ (cm <sup>-3</sup> ambient $\times 10^{-3}$ )					$N_{.25}^\dagger$ (cm <sup>-3</sup> ) Ambient $\times 10^{-3}$	$f_m(z)^\ddagger$ (m <sup>-1</sup> sr <sup>-1</sup> $\times 10^{-9}$ )	$f_p(z)^\S$ (m <sup>-1</sup> sr <sup>-1</sup> $\times 10^{-9}$ )	R(z)**
		r =								
		(0.25-0.35 $\mu$ m)	(0.35-0.70 $\mu$ m)	(0.70-1.50 $\mu$ m)	(1.50-2.50 $\mu$ m)	( $\geq$ 2.5 $\mu$ m)				
(1)	(2)	(3)	(4)	(5)	(6)	(7)	(8)	(9)	(10)	(11)
2117-2155	9.5	5.42	3.25	0.667	0.050	0.051	9.44	197	0.08 - 0.76	1.000-1.004
2155-2218	10.7	28.60	18.10	2.445	0.012	0.011	49.27	170	0.42 - 4.0	1.002-1.024
2227-2249	12.2	51.35	24.48	2.538	0.009	0.007	78.38	142	0.68 - 6.3	1.005-1.044

\* Measured by Royco particle counter on Convair 990. Results at 9.5 km are the average of three convective ten-minute samples. At the other levels they are the average of two such samples.

$^\dagger$  Sum of Columns 3-7.

$^\ddagger$  Computed from Oakland radiosonde profile, 22 January 1974, 0500 PDT.

$^\S$  Range of values computed from  $N_{.25}$  (Column 8) assuming haze H or haze L size distribution, and refractive index ranging between 1.31 and 1.54

\*\*  $1.0 + (\text{Column } 10 \div \text{Column } 9)$ .

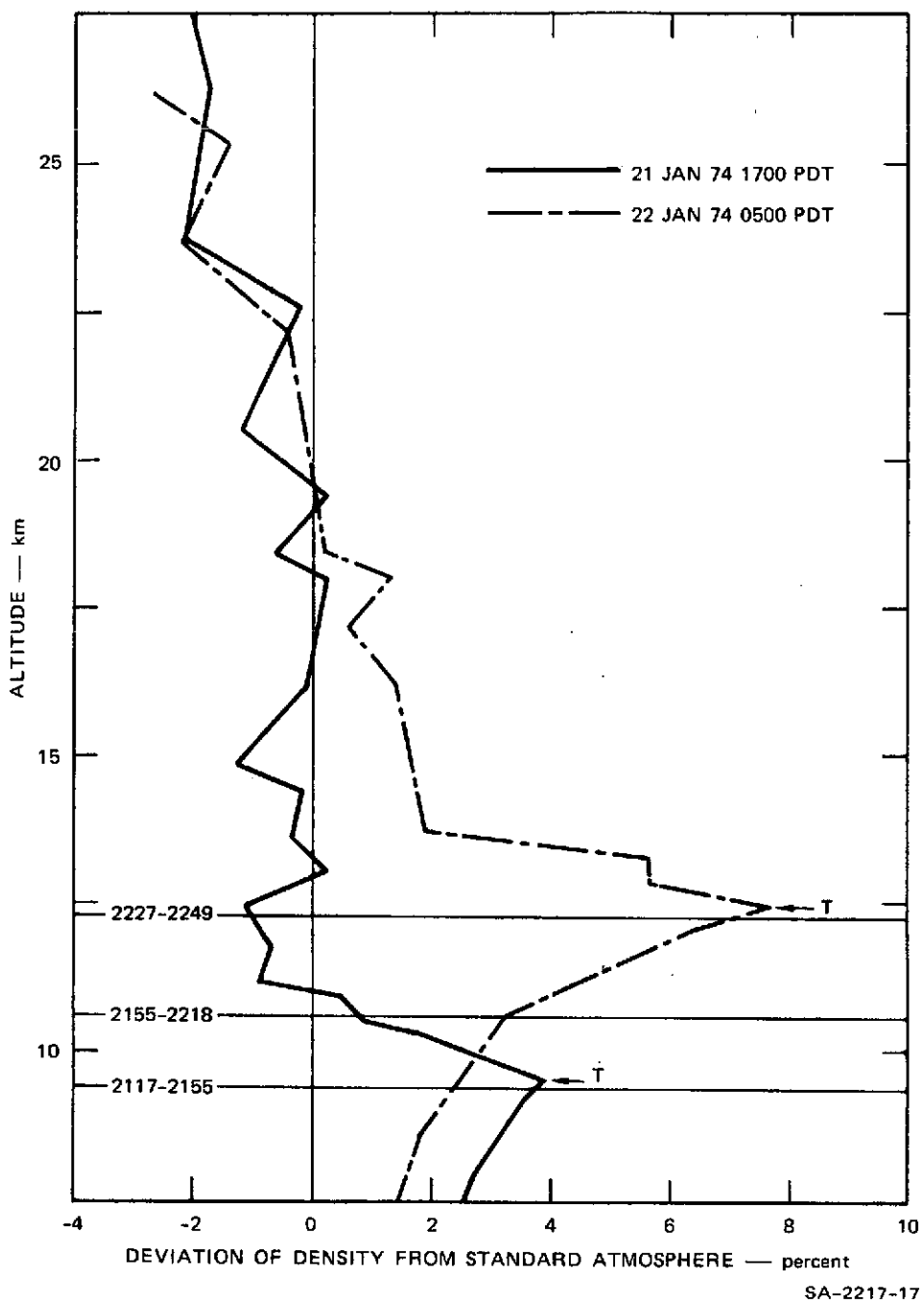


FIGURE 10 MOLECULAR DENSITY PROFILES OBTAINED BY OAKLAND  
 RADIOSONDE SOUNDINGS, NIGHT OF 21-22 JANUARY 1974  
 Horizontal lines give Convair 990 flight altitudes and times (PDT).  
 Arrows indicate tropopause heights.

contribution to the lidar return signal), those measurements are not discussed here.

Figure 10 shows molecular density profiles (presented as percentage deviations from the midlatitude spring/fall U.S. standard atmosphere) obtained from the Oakland radiosonde soundings made just before and after the overflight. As can be seen, the night of 21-22 January was characterized by rapid and significant change at the upper flight altitudes. A layer of dense, cold air moved into the flight region during the 12-hour period between radiosonde soundings, causing the tropopause to rise from 9.5 to 12.4 km. The rapid decrease in temperature at the upper flight altitude led to the formation of a cirrus cloud between 0400 and 0430 PDT, after the flight had been completed (see below). (Again, add seven hours to PDT times to obtain GMT times.)

Because of the changing altitude of the tropopause, it is not clear whether the Convair 990 actually penetrated into the stratosphere in a strict sense. However, it is certain that the aircraft was not high enough to sample particles from the Junge layer of stratospheric particles. In terms of a lidar/in situ experiment, therefore, the Convair 990 overflight did not provide comparative information on the stratospheric aerosol per se. However, numerous balloon-borne photoelectric particle counter measurements by the University of Wyoming (see, e.g., Hofmann et al., 1973) have shown that typically there is a minimum in particle concentration near the tropopause. Furthermore, the matching level used

in our lidar profile analyses usually is also found near the tropopause. Therefore the Convair 990 comparative experiment primarily provided a test of the validity of the clean air assumption used in the matching method of lidar analysis.

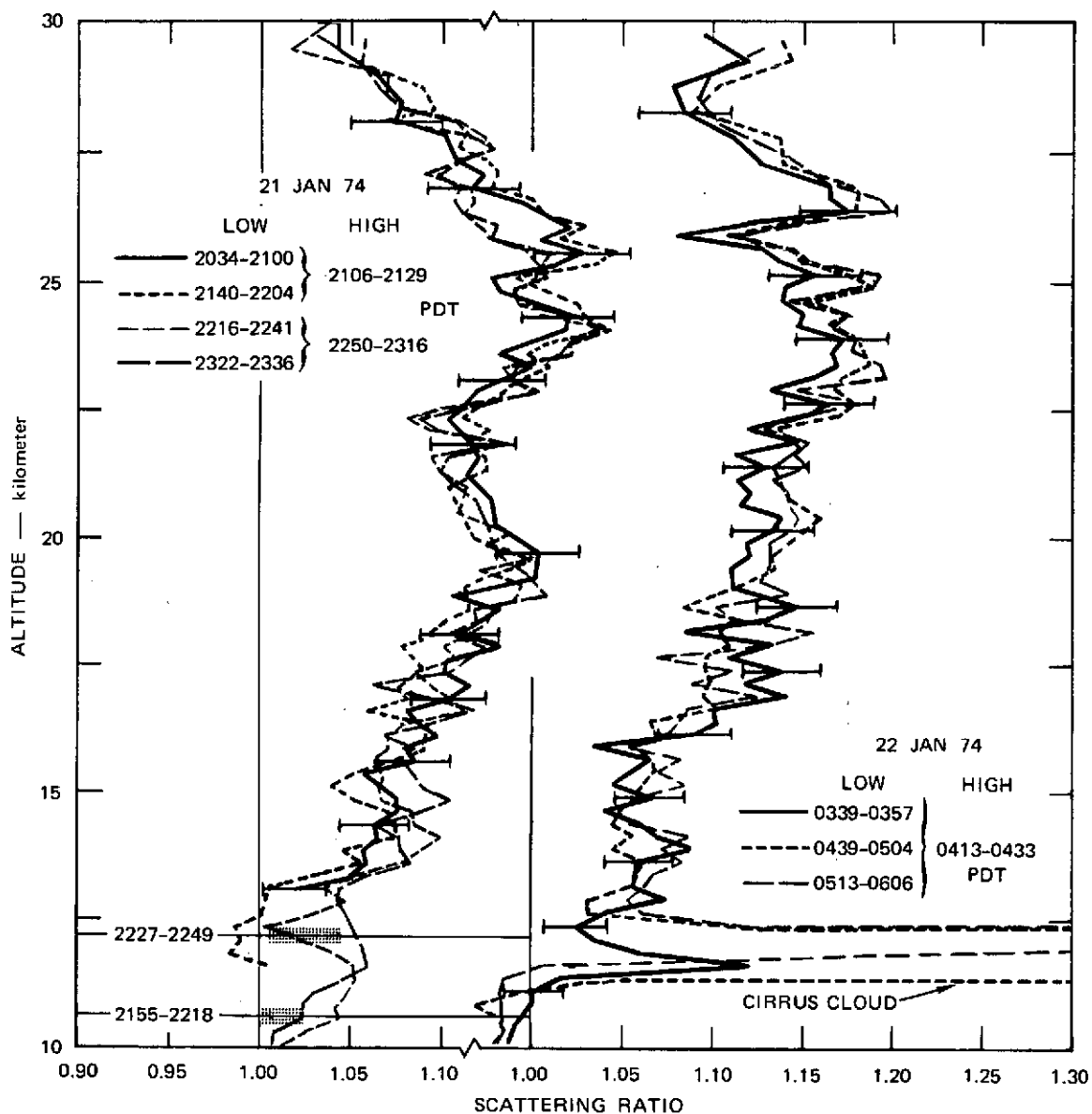
We performed this test by computing expected lidar scattering ratios from the aircraft particle-counting data. This computation requires information on both particle size distribution and particle refractive index. Particle size distribution histograms for particles with radius  $r \geq 0.25 \mu\text{m}$  can be drawn from the data in Table 6. For all three flight levels these histograms fall in between histograms computed from the analytical size distributions haze L and haze H of Deirmendjian (1969), but more closely approximate haze L than haze H, especially for the lower flight levels ( $z = 9.5$  and  $10.7$  km). The size distributions, of course, should not necessarily be expected to approximate haze H (cf. the preceding sub-section), because the sampled particles were not from the Junge layer.

The tropospheric nature of the sampled particles also makes their refractive index uncertain. Reasonably expected values could range from 1.31 (ice) to 1.54 (silicate), with possibly nonzero imaginary components. Therefore, we have computed particulate backscattering coefficients  $f_p$  for a wide range of refractive indices and size distributions, including the extremes noted above. The ranges of resulting values, for the numbers of particles sampled at the three flight levels, are shown

in Table 6, along with the corresponding scattering ratios. Fortunately, as can be seen, the numbers of sampled particles were so small at all levels that the ambiguity in particle composition and size distribution produces only moderate ambiguity in computed scattering ratios. Within the lidar measurement accuracy, the computed scattering ratios at 9.5 and 10.7 km are unity--i.e., the particulate content there is negligible from the standpoint of lidar scattering ratio measurements.

Lidar observations were made on the night of the Convair 990 overflight between 2034 and 2336 PDT and again between 0339 and 0513 PDT. The observations were made in alternating low- and high-sensitivity modes as described in Section 2(b). The resulting composite profiles of scattering ratio, and the times of acquisition of low-altitude (low-sensitivity) and high-altitude (high-sensitivity) portions are shown in Fig. 11. The molecular density profile used in computing these ratio profiles is that given by the 22 January 1974 0500 PDT Oakland radiosonde sounding, shown in Fig. 10. Generally speaking, the composite profiles below 20 km are determined only from the low-sensitivity observations, and the composite profiles above 20 km are an error-weighted average of the indicated low- and high-sensitivity profiles. The low-altitude cutoff of the low-sensitivity runs was gradually extended downward, from 13.0 to 8.0 km, as the night progressed.

As can be seen from Fig. 11, the structure of the stratospheric aerosol layer between 15 and 27 km remained quite stable throughout the



SA-2217-16

FIGURE 11 PROFILES OF SCATTERING RATIO OBSERVED BY LIDAR ON NIGHT OF 21-22 JANUARY 1974.

Horizontal lines give Convair 990 flight altitudes and times (PDT). Dark rectangles on flight lines give range of possible scattering ratios computed from aircraft particle-counting data.

observation period. This type of stability is typical of our observations (see, e.g., Russell et al., 1973a). However, below 13 km continually changing conditions are evident, notably in the form of a peak in scattering ratio that grows in both magnitude and altitude as the night progresses. Such a peak could result from an increase in either atmospheric density or particulate content, and it is probable that in this case both mechanisms were operative. For example, the radiosonde soundings (cf., Fig. 10) show that the molecular density at 12.5 km increased by at least 9 percent between soundings, while it is clear from the late lidar observations that a layer of cirrus formed after 0400 PDT.

This type of rapid and significant change in molecular density between afternoon and morning radiosonde soundings is not typical of conditions during the 1972-74 series of lidar observations, but it introduces an ambiguity into interpretation of scattering ratios near the tropopause for this particular observation. Nevertheless, the following comparison between lidar-measured and aircraft-inferred scattering ratios can be made. The aircraft-inferred scattering ratios for the two upper flight levels, as given in Table 6, are plotted in Fig. 11 as dark rectangles at the flight altitude. As can be seen, only one aircraft measurement (that at 12.2 km) was actually made concurrent with a lidar observation at its altitude. For that case there is good agreement between the lidar-measured scattering ratio and the range of values computed from the aircraft data. The aircraft measurement at 10.7 km was made almost

entirely before the lidar observations were extended downward to that level. As can be seen, the first lidar profile to extend down to 10.7 km gives a scattering ratio that exceeds the range of aircraft-inferred values by more than one error bar. However, given the difference in time between the two observations, the changes in atmospheric density (and possibly particulate content) that were occurring, and the possibility that the peak in lidar scattering ratio results from atmospheric density effects, the agreement is as good as can be expected.

Because of rapidly changing atmospheric density near the tropopause and the low upper limit on flight altitudes, therefore, the 21 January 1974 Convair 990 overflight did not provide an optimal comparative lidar/direct-sampling experiment. It did, however, provide additional support for the validity of the matching method of lidar profile analysis, since a rather extensive clean layer was found by the aircraft, and the altitude of this layer corresponded to the altitude located by the standard matching analysis method (see Section 3a). It should of course be emphasized that the results obtained on 21 January 1974 strictly apply only to that date, and do not necessarily imply that there is a clean ( $f_p/f_m \leq 0.01$ ) layer near the tropopause on all nights in all seasons. More extensive data obtained by the University of Wyoming (see, e.g., Hofmann et al., 1973a,b), have shown fluctuating particle numbers with a possible seasonal dependence at the concentration minimum near the tropopause. Further analysis of the balloon data to specifically determine their implications

for lidar-measured scattering ratios is recommended. Moreover, the possible presence of optically significant numbers of particles that are smaller than the detection thresholds ( $r = 0.25$  and  $0.15 \mu\text{m}$ , respectively) of the Royco and Wyoming photoelectric particle counters should also be investigated. The presence of such particles has been indicated in the past, for example by the measurements of de Bary and Rössler (1966).

(iii) U-2 Overflight. On the night of 18 March 1974, a U-2 aircraft from NASA Ames Research Center (ARC) in Mountain View, California, made passes over the SRI lidar site at altitudes of 19.5 and 20.1 km. The aircraft carried a particle-collection device provided by Guy Ferry of ARC. Particles collected at both flight altitudes were subsequently returned to ARC where they were analyzed using a scanning electron microscope, as described by Farlow et al. (1973). This type of analysis provides information on particle size distribution and also, through X-ray emission analysis, on particle elemental composition.

Lidar observations were also made on the night of the U-2 flight, and the resulting profiles of scattering ratio and particulate back-scattering coefficient are included in Figs. 3 and 4. Comparative analysis of the U-2 and lidar data is not yet complete, and the results will be described in a future publication.

## 5. DISCUSSION OF ATMOSPHERIC OBSERVATIONS

The profiles of scattering ratio obtained in this study show the Junge (or "20-km") layer of particles to be a quasi-permanent feature of the lower stratosphere over Menlo Park, California ( $37.4^{\circ}\text{N}$ ,  $122.2^{\circ}\text{W}$ ), from October 1972 to March 1974. This major peak of scattering excess is apparent in all of our observations, although it has displayed significant variations in both magnitude and shape. With two exceptions, the maximum value of the scattering ratio has ranged between 1.07 and 1.22. In one exceptional case (11 September 1973) the layer was very broad, and the maximum scattering ratio in the main peak was only 1.05. Even in this case, the presence of a particulate excess in stratospheric backscattering was evident beyond the combined observational uncertainties.

The observed scattering ratios show that in general the maximum particulate contribution to stratospheric backscattering at the ruby wavelength ( $\lambda = 694.3 \text{ nm}$ ) was only about 10 to 15 percent of the molecular contribution. This may be compared with particulate contributions that were approximately 60 to 120 percent of the molecular backscattering contribution during the 1964-65 observations of Grams and Fiocco (1967). The lidar observations thus show a decline in particulate backscattering by nearly an order of magnitude over the ten-year period. This decline has been previously noted by many other investigators, who have attributed

it to the gradual removal of particles that resulted from the eruption of the volcano Agung on Bali in March 1963. More detailed and extensive data, including other lidar observations (summarized by Fox et al., 1973), the twilight photometry of Volz (1969, 1970, 1972, 1973), and the balloon-borne particle counting observations of the University of Wyoming group (e.g., Hofmann et al., 1972, 1973) have shown that numerous short-term fluctuations are imposed on this general decline. Careful measurements of sulfate concentration and sulfur isotope ratios by Castleman et al. (1973a,b), have shown that at least part of these fluctuations is due to major volcanic eruptions subsequent to the Agung event, notably Taal (1965), Awu (1966), and Fernandina (1968).

Above the major Junge layer, average particulate backscattering is smaller, but its relative variations are considerably larger, and may occur in response to factors other than volcanic activity. For example, in our earliest observations (23 October 1972 to 11 December 1973) there appears to be a well-defined particulate layer between 24 and 27 km that decreased in altitude with time, and finally merged with the main layer or disappeared by January 1973. Lidar observations in Japan by Hirono et al. (1972) also indicated large particulate scattering above the main layer at this time, and those observers speculated that its presence could be due to an influx of dust from the comet Giacobini-Zinner. Maximum scattering ratios observed by the Japanese group greatly exceeded any ever observed in the present study.

Following the autumn 1972 appearance of particulate content between 25 and 30 km, January 1973 was characterized by a complete absence of particulate backscattering in that region, and by a major Junge peak that was more sharply-defined (i.e., narrow) than in most other observations. The coincidence of this behavior with the time of a sudden stratospheric warming has been noted above and probably bears further study.

After January 1973 significant particulate backscattering at 30 km was noted intermittently throughout the remainder of the study. Scattering ratio profiles were frequently similar to the average profiles of Fox et al. (1973), in exhibiting a very broad maximum that did not appreciably decline near 30 km. Similar structure has also been noted by Volz (1971).

In our later observations, for which profiles of scattering ratio were obtained both above and below the tropopause, a relative minimum in scattering ratio was invariably observed near, but not necessarily at, the tropopause. A similar minimum in particle number per microgram of air has also been consistently observed by the University of Wyoming balloon soundings.

After 4 January 1974 the altitude of the maximum scattering ratio in all our observations ranged between 21 and 23 km. Recent lidar and balloon observations in Wyoming (42°N) and Colorado (40°N)--Dynatrend 1973--have shown the maximum to be somewhat lower, at about 18 km. In the past, latitudinal variations in the altitude of the main aerosol peak have been

noted to follow similar latitudinal changes in tropopause height (Grams and Fiocco 1967), and thus similarly, the present longitudinal difference between California coastal and continental layer heights may be at least partially explained by tropopause height differences. However, seasonal-mean tropopause heights at Menlo Park and Wyoming-Colorado do not appear to differ by more than 2 or 3 km, and thus other mechanisms, for example in stratospheric zonal and vertical flow, should be investigated to explain this difference in peak altitudes.

We have also inspected our data for temporal correlations between tropopause height and that of the peak and centroid in scattering ratio. In general, if such a correlation exists, it is very weak. That is, the altitude of the main peak does not appear to strongly follow variations in the tropopause altitude at Menlo Park. This lack of correlation is in accord with previous results obtained by direct sampling (Junge and Manson 1961) and lidar observations (Grams and Fiocco 1967) in Massachusetts.

Because of increasing atmospheric density with decreasing height, particulate backscattering below the peak in scattering ratio  $R$  usually makes a major contribution to the vertically-integrated particulate backscattering  $(\int f_p(z) dz = \int f_m(z) [R(z) - 1] dz)$  above the tropopause. This fact, coupled with the fact that temporal variations in aerosol layer altitudes do not tend to follow temporal variations in tropopause height, means that a rising tropopause frequently results in a decrease

in integrated particulate content above the tropopause. A resulting negative correlation between tropopause height and integrated particle number above the tropopause has been noted by Hofmann et al. (1973), and appears also to be present in our data after May 1973, when observations consistently extended below the tropopause.

The particulate optical thicknesses  $\Delta\tau_p$  obtained from our lidar observations by using a model value for the backscattering phase function  $P(\pi)$  are nearly an order of magnitude smaller than the values of the Elterman (1968) model. Since the model values are based on searchlight measurements made in 1964 and 1965, when effects of the Agung eruption were still significant, this discrepancy is not surprising, and in fact agrees rather well with the 1964-74 trend in lidar backscattering ratios mentioned above. More difficult to explain is the fact that the present lidar-determined optical thicknesses are also a factor of four to ten smaller than those determined by searchlight measurements made in October and November of 1970 (Elterman et al., 1973).

One possible reason for this discrepancy is of course the choice of backscattering phase function used in converting our backscattering measurements to extinction values. The value  $[P(\pi)/4\pi = 0.0132]$  that we have used is appropriate if the optical properties of the present stratospheric particles are similar to those of homogeneous spheres of 75 percent concentrated sulfuric acid, and if their size distribution approximates the Deirmendjian haze H distribution. As shown in Section 4(e),

such an optical model appears to be consistent with a number of recent stratospheric measurements, but its validity has not been conclusively demonstrated, especially over time periods of several years and altitude ranges that include the bulk of the Junge layer. It is important to note, however, that agreement between the present lidar measurements and the 1970 searchlight measurements requires a backscattering phase function that is a factor of four to ten smaller than the model value we have used. Such a small value for the backscattering phase function does not occur for any of the wide range of optical models shown in Table 3, all of which assume spherical particles of nonabsorbing material. Thus agreement between the present lidar measurements and the 1970 searchlight measurements evidently requires that the optically significant stratospheric particles be highly aspherical (Holland and Gagne 1970) or absorptive in the visible (Grams et al., 1974), or both. While more measurements are required to conclusively assess this possibility, it does not appear to be consistent with current measurements.

Before leaving the question of the backscattering phase function, we note that the conversion of raw searchlight scattering measurements to values of optical thickness also requires the assumption of a scattering phase function in the angular region  $\theta \approx 80^\circ$  to  $110^\circ$  (Elterman and Campbell 1964, Elterman 1966). The phase function actually used in reducing the 1964-65 and 1970 searchlight measurements (Reeger and Siedentopf 1946) has a backscattering value that is larger than our

assumed value, and would thus produce even smaller lidar-derived optical depths.

A more likely reason for the discrepancy between the lidar- and the searchlight-derived optical thicknesses is the different time periods at which the measurements were made. Elterman (1973) states that the 1970 measurements are representative of a background nonvolcanic stratosphere, but other measurements indicate that particulate content has continued to decline since that time. Specifically we note the time series of lidar observations summarized by Fox et al. (1973), and the twilight scattering measurements of Volz (1970, 1972, 1973). The latter measurements indicated a temporary increase in particulate content (over Boston, Massachusetts) in late 1970 (including October and November), and a general decline thereafter, interrupted only by a brief but major increase in October 1971.

However, the fact that the searchlight measurements show only a 17 percent decline in stratospheric particulate optical depth between 1964-65 and 1970 makes it appear worthwhile to investigate other possible differences between the lidar and searchlight measurements. A factor that bears mention is the normalization of the lidar and searchlight measurements. Both techniques obtain particulate scattering values by referencing measured intensities to those expected from a purely gaseous atmosphere. The searchlight measurements provide a scattering profile that extends upward from an altitude of only a few kilometers. The 1970

profile of turbidity [ $t(z) \equiv \beta_p(z)/\beta_m(z)$ ] obtained in this manner exceeds 0.5 for all altitudes between 10 and 27 km. Thus, the 1970 searchlight measurements imply that there was no clean level in the stratosphere below 27 km (the upper limit of measurements). In fact, at 10 km the searchlight-derived turbidity [ $t(10) = 0.9$ ] is two-thirds of the value [ $t(16) = 1.5$ ] at the peak of the aerosol layer. This is very different from the lidar measurements, where the backscattering mixing ratio,  $R(z) - 1$ , at 10 km is generally negligible compared to its value at the peak of the layer. Since the searchlight measurements cover a much larger altitude range than do the lidar measurements, this immediately raises the possibility that the lidar measurements have neglected a sizeable particulate contribution at the normalization level where  $R$  is assumed to equal unity. However, unless there is a very large (optically significant) number of small particles with radius  $< 0.25 \mu\text{m}$  (which would not be seen by an optical particle counter), this possibility is not consistent with the essentially clean layer found by the Convair 990 on 21 January 1974 [see Section 4(e)(ii)], nor with the number mixing ratios (particle number per microgram of air) observed by the University of Wyoming balloon flights, where the minimum value (near the tropopause) is invariably a factor of five, and typically a factor of ten or more, less than the peak value. These interesting discrepancies between the lidar and searchlight measurements bear further investigation, ideally including joint comparative measurements involving direct sensors as well.

After June 1973, when the lidar measurements consistently extended as low as the tropopause<sup>9</sup> and below, the measured particulate optical thicknesses (cf. Fig. 6) do not show any overall increasing or decreasing trend with time. This may possibly indicate that a background level in stratospheric particulate content was achieved during this time. However, the observation period of the apparently stable data is only eight months. Extended observations will be required to ascertain whether this data sample is representative.

## 6. NOTES AND RECOMMENDATIONS ON THE LIDAR OBSERVATIONAL TECHNIQUE

As a remote sensing device, the lidar naturally suffers from several deficiencies when compared to in situ devices for measuring stratospheric particulate content. It cannot provide information on particle chemical composition, or, if restricted to single-wavelength operation, on particle size distribution. Moreover, the optical quantities that it measures cannot be unambiguously converted to particle number or mass without auxiliary information on particle composition, shape, and size distribution. Nevertheless, the lidar has several advantages over direct sensors that make it a useful adjunct to direct (and other remote) sensors in stratospheric studies. These advantages include its ability to rapidly and continuously observe stratospheric regions of large vertical extent, the fact that it does not alter the quantities that it is observing, and its significantly lower cost per observation, which permits broad coverage in time and possible network operation. Lidar observations are thus valuable sources of information on the stratospheric aerosol, and are of especial value in extending and complementing available in situ measurements, as shown by the discussion which follows.

In the absence of auxiliary data to make conversions, the profiles of scattering ratio and particulate backscattering coefficient directly provided by the lidar immediately reveal the presence, altitude-dependence,

backscattering strength, and variability (in space and time) of stratospheric aerosol layers. These profiles have been used to document the general decline in stratospheric particulate content between 1964 and 1974. In the present study they have also been used to study the changing character of the stratospheric aerosol in relation to tropopause heights, stratospheric winds, and a sudden stratospheric warming. These studies illustrate the value of the lidar in investigations that require data with a coverage in time and altitude that would be impossible or extremely expensive to achieve with direct sensors. In the future this capability could be further exploited by operating lidars in a monitoring fashion, utilizing their measurements to select optimum times and altitudes for more detailed direct sampling studies, for example during times of unusual or otherwise interesting behavior of the lidar profiles.

It should also be pointed out that the nature of the fundamental lidar data profiles makes them potentially useful in future modeling studies. A fundamental result of dynamic, radiative, and photochemical models of the stratosphere is a set of vertical profiles, or two-dimensional contour plots, of the mixing ratio of the modeled constituent (see, e.g., Rao 1973; Rao and Christie 1973). Model development and verification studies therefore require measurements of such mixing ratio profiles or contour plots, preferably obtained by a single measurement method, and at a single time or averaged over a suitable time period. Lidar-measured profiles of backscattering mixing ratio,  $R(z) - 1$ ,

would thus be well-suited to the development of aerosol formation and transport models. In the past such models have not been attempted because of the complexity of aerosol formation processes and our limited understanding of them. However, as pointed out by Castleman (1974), stratospheric aerosol chemistry appears to be a fruitful area for future research, and the development of crude models may not be far in the future. Similarly, the shape of lidar scattering ratio profiles could also possibly be used to determine vertical eddy diffusion coefficients in the stratosphere (see, e.g., Wofsy and McElroy 1973; Clemesha and Nakamura 1972).

In the types of study just mentioned, information is obtained directly from the fundamental lidar data, i.e., vertical profiles of the scattering ratio and particulate backscattering coefficient. The accuracy of these profiles has been supported by several recent lidar/direct-sensing comparisons, including the Laramie Comparative Experiment (Dynatrend 1973; Fernald et al., 1973; and Melfi et al., 1973) and the WB-57F and Convair 990 overflights described in Section 4(e). Moreover, the simultaneous data on particle physical, chemical, and light-scattering characteristics obtained in these comparative experiments have helped to define the range of possible conversion factors  $[\tilde{f}_p, \hat{f}_p, P(\pi)]$  to be used in converting lidar measurements to particle mass, number density, and optical thickness. Continuing direct-sampling studies, which more accurately determine the nature and variability of the stratospheric particles, should lead to

a more accurate and reliable definition of these conversion factors. If the variability of these conversion factors is shown to be small, then eventually it will be possible to obtain reliable inferences of the mass, number density, and optical thickness of the stratospheric aerosol from lidar measurements on a regular basis. This is not to say that such conversion factors, once determined, would not change over long time periods (years or decades) or in response to obvious external influences, such as volcanic eruptions or aircraft operations. Direct-sampling measurements could provide periodic "calibrations" of the conversion factors while a network of lidars could be used to perform routine monitoring.

In the present study, sequential observations with ruby and dye lasers showed a wavelength-dependence of stratospheric scattering that is consistent with the presence of particles having a size distribution in agreement with previous experimental and theoretical studies. Future continuation of such multiple-wavelength observations is recommended, using more powerful dye lasers to provide improved accuracy. Such studies not only would provide information on particle size distributions, but also could be used to separate the effects of particle concentration and anomalous molecular density variations on measured scattering ratio profiles. As shown by the data of 21-22 January 1974 [Section 4(e)(iii)], such occasional variations near the tropopause may confuse the interpretation of lidar profiles measured between radiosonde soundings, especially

when particulate concentrations are small, as they have been for the past several years.

A more direct resolution of the effects of molecular density variations on lidar-measured scattering ratio profiles could be provided by concurrent lidar measurements of the Raman-scattering profile of nitrogen molecular density. Such measurements, which have been conducted in the troposphere for several years, were recently extended into the stratosphere (up to ~45 km) by Garvey and Kent (1974). If such measurements can be refined to a relative accuracy of one or two percent by using increased laser power and receiver area, they would permit the acquisition of accurate scattering ratio profiles without the need for concurrent radiosonde ascents, even at times of rapidly changing molecular density near the tropopause. The development of such coordinated Raman/elastic scattering stratospheric lidar systems is therefore to be encouraged.

# REFERENCES

- Bartusek, K., Gambling, D. J., and Elford, W. G. 1970 "Stratospheric aerosol measurements by optical radar," J. Atmos. Terr. Phys., 32, pp. 1535-1544.
- Bigg, E. K., Kviz, Z., and Thompson, W. J. 1971 "Electron microscope photographs of extraterrestrial particles," Tellus, 23, pp. 247-260.
- Briehl, Daniel, NASA-Lewis Research Center, Cleveland, Ohio 1974 Private communication.
- Cadle, R. D. 1972 "Composition of the stratospheric 'sulfate' layer," EOS Trans. Am. Geophys. Union, 53, pp. 812-820.
- Castleman, A. W., Jr. 1974 "Nucleation processes and aerosol chemistry," Space Sci. Rev., 15, pp. 547-589.
- Castleman, A. W., Jr., Munkelwitz, H. R., and Manowitz, B. 1973a "Contribution of volcanic sulphur compounds to the stratospheric aerosol layer," Nature, 244, pp. 345-346.
- Castleman, A. W., Jr., Munkelwitz, H. R., and Manowitz, B. 1973b Tellus (in the press).
- Clemensha, B. R., Kent, G. S., and Wright, R.W.H. 1966 "Laser probing of the lower atmosphere," Nature, 209, pp. 184-185.
- Clemensha, B. R., and Nakamura, Y. 1972 "Dust in the upper atmosphere," Nature, 237, pp. 328-329.
- Clemensha, B. R., and Rodrigues, S. N. 1971 "The stratospheric scattering profile at 23° South," J. Atmos. Terr. Phys., 33, pp. 1119-1124.

- |  |      |  |
|--|------|--|
| Cohen, A., and Graber, M.  | 1973 | "Stratospheric aerosol lidar measurements over Jerusalem," Fifth Conference on Laser Radar Studies of the Atmosphere, Williamsburg, Virginia.  |
| Collis, R.T.H., and Ligda, M.G.H.                                | 1966 | "Note on lidar observations of particulate matter in the stratosphere," <u>J. Atmos. Sci.</u> , <u>23</u> , pp. 255-257.   |
| Collis, R.T.H., Viezee, W., Hake, R. D., Jr., and Russell, P. B. | 1973 | "Lidar measurements of the variability of stratospheric particulates," AIAA/AMS International Conference on Environmental Impact of Aerospace Operations in the High Atmosphere, Denver, Colorado. |
| Cronin, J. F.  | 1971 | "Recent volcanism and the stratosphere," <u>Science</u> , <u>172</u> , pp. 847-849.  |
| de Bary, E., and Rössler, F.                                     | 1966 | "Size distributions of atmospheric aerosols derived from scattered radiation measurements aloft," <u>J. Geophys. Res.</u> , <u>71</u> , pp. 1011-1016.   |
| Deirmendjian, D.   | 1969 | <u>Electromagnetic scattering on spherical polydispersions</u> , American Elsevier, New York.  |
| Deirmendjian, D.   | 1972 | "On volcanic and other particulate turbidity anomalies," paper no. P-4782, available from the author, The Rand Corporation, Santa Monica, California.  |
| Dynatrend, 1973.   | 1973 | "Laramie comparative experiment, data report and preliminary report of conclusions," edited by Dynatrend, Inc.   |
| Elterman, L.   | 1966 | "Aerosol measurements in the troposphere and stratosphere," <u>Appl. Opt.</u> , <u>5</u> , pp. 1769-1776.  |
| Elterman, L.   | 1968 | "UV, visible and IR attenuation for altitudes to 50 km, 1968," AFCRL-68-0153, Environmental Research Paper No. 285.  |

- Elterman, L., and Campbell, A. B. 1964 "Atmospheric aerosol observations with searchlight probing," J. Atmos. Sci., 21, pp. 457-458.
- Elterman, L., Toolin, R. B., and Essex, J. D. 1973 "Stratospheric aerosol measurements with implications for global climate," Appl. Opt., 12, pp. 330-337.
- Farlow, N. H., Ferry, G. V., and Lem, H. Y. 1973 "Analysis of individual particles collected from the stratosphere," Space Res., 13, in press.
- Fernald, F. G., Schuster, B. G., and Frush, C. L. 1973 "Comparison of lidar aerosol measurements and direct particulate sampling," Fifth Conference on Laser Radar Studies of the Atmosphere, Williamsburg, Virginia, Conference Abstracts, pp. 31-33.
- Ferry, G., NASA Ames Research Center, Mountain View, California. 1974 Private communication.
- Fiocco, G., and Grams, G. 1964 "Observations of the aerosol layer at 20 km by optical radar," J. Atmos. Sci., 21, pp. 323-324.
- Fiocco, G., and Grams, G. 1966 "Observations of the upper atmosphere by optical radar in Alaska and Sweden during the summer 1964," Tellus, 18, pp. 34-38.
- Fox, R. J., Grams, G. W., Schuster, B. G., and Weinman, J. A. 1973 "Measurements of stratospheric aerosols by airborne laser radar," J. Geophys. Res., 78, pp. 7789-7801.
- Friedlander, S. K. 1961 "Theoretical considerations for the particle size spectrum of the stratospheric aerosol," J. Meteor., 18, pp. 753-759.
- Friend, J. P., Leifer, R., and Trichon, M. 1973 "On the formation of stratospheric aerosols," J. Atmos. Sci., 30, pp. 465-479.
- Garvey, M. J., and Kent, G. S. 1974 "Raman backscatter of laser radiation from the stratosphere," Nature, 248, pp. 124-125.

- Giauque, W. F.,  
Hornung, E. W.,  
Kunzler, J. E.,  
and Rubin, T. R. 1960 "The thermodynamic properties of aqueous sulfuric acid solutions and hydrates from 15 to 300° K," J. Amer. Chem. Soc., 82, p. 62.
- Grams, G. W. 1966 "Optical radar studies of stratospheric aerosols," Thesis, Dept. of Meteorology, Mass. Inst. of Tech., 113 pp.
- Grams, G., and Fiocco, G. 1967 "Stratospheric aerosol layer during 1964 and 1965," J. Geophys. Res., 72, pp. 3523-3542.
- Grams, G. W., Bilford, I. H., Jr.,  
Gillette, D. A.,  
and Russell, P. B. 1974 "Complex index of refraction of airborne soil particles," J. Appl. Meteor., 13, to be published.
- Gray, D. E. 1963 American Institute of Physics Handbook, McGraw-Hill, New York, pp. A-91.
- Gruner, P., and Kleinert, H. 1927 "Die Dämmerungserscheinungen," Probleme der Kosmischen Physik, 10, Henri Grand, Hamburg, pp. 1-113.
- Hirono, M., Fujiwara, M., Uchino, O. and Itabe, T. 1972 "Observations of aerosol layers in the upper atmosphere by laser radar," Rep. of Ionos. and Space Res. in Japan, 26, pp. 237-244.
- Hofmann, D. J., Rosen, J. M., Pepin, T. J., and Kroening, J. L. 1972 "Global measurements of stratospheric aerosol, ozone, and water vapor by balloon-borne sensors," Second Conference on CIAP, Cambridge, Mass., Conference Proceedings, pp. 23-33.
- Hofmann, D. J., Rosen, J. M., and Pepin, T. J. 1973 "The global stratospheric aerosol burden," paper presented at the Fifth Conference on Laser Radar Studies of the Atmosphere, 4-6 June 1973, Williamsburg, Virginia.
- Holland, A. C., and Gagne, G. 1970 "The scattering of polarized light by polydisperse systems of irregular particles," Appl. Opt., 9, pp. 1113-1121.

- Hoxit, L. R., and Henry, R. M. 1973 "Diurnal and annual temperature variations in the 30-60 km region as indicated by statistical analysis of rocketsonde temperature data," J. Atmos. Sci., 30, pp. 922-932.
- Junge, C. E. 1963 Air chemistry and radioactivity, Academic Press, New York, 382 pp.
- Junge, C. E., and Manson, J. E. 1961a "Stratospheric aerosol studies," J. Geophys. Res., 66, pp. 2163-2182.
- Junge, C. E., Chagnon, C. W., and Manson, J. E. 1961b "Stratospheric aerosols," J. Meteor., 18, pp. 81-108.
- Kent, G. S., Clemensha, B. R., and Wright, R. W. 1967 "High altitude atmospheric scattering of light from a laser beam," J. Atmos. Terr. Phys., 29, p. 169.
- Kent, G. S., and Wright, R.W.H. 1970 "A review of laser radar measurements of atmospheric properties," J. Atmos. Terres. Phys., 32, pp. 917-943.
- Lenhard, R. W. 1973 "A revised assessment of radiosonde accuracy," Bull. Am. Met. Soc., 54, pp. 691-693.
- McCormick, M. P., Lawrence, J. D., Jr., and Crownfield, F. R., Jr. 1968 "Mie total and differential backscattering cross sections at laser wavelengths for Junge aerosol models," Appl. Opt., 7, pp. 2424-2425.
- Melfi, S. H., Northam, G. B., McCormick, M. P., Rosen, J. M., Pepin, T. J., and Hofman, D. H. 1973 "Comparison of lidar and in situ measurements of stratospheric aerosols," Fifth Conference on Laser Radar Studies of the Atmosphere, Williamsburg, Virginia, Conference Abstracts, p. 35.
- Mossop, S. C. 1964 "Volcanic dust collected at an altitude of 20 km," Nature, 203, pp. 824-827.
- Neumann, J. 1973 "Radiation absorption by droplets of sulfuric acid-water solution and by ammonium sulfate particles," J. Atmos. Sci., 30, pp. 95-100.

- Ottway, M. T. 1972 "Laser radar observations of the 20-km aerosol layer," paper presented at Fourth Conference on Laser Radar Studies on the Atmosphere, Group on Laser Atmos. Probing, Tucson, Arizona.
- Pilipowskyj, S., Weinman, J. A., Clemensha, B. R., Kent, G. S., and Wright, R. W. 1968 "Investigation of the stratospheric aerosol by infrared and lidar techniques," J. Geophys. Res., 73, p. 7553.
- Quiroz, R. S. 1973 "The abnormal stratosphere studied with the aid of satellite radiation measurements," Paper for AIAA/AMS International Conference on the Environmental Impact of Aerospace Operations in the High Atmosphere, Denver, Colorado.
- Rao, V.R.K. 1973 "Numerical experiments on the steady-state meridional structure of the stratosphere, incorporating radiative heating and ozone photochemistry," Mon. Wea. Rev., 101, pp. 510-527.
- Rao, V.R.K., and Christie, A. D. 1973 "The effects of water vapor and oxides of nitrogen on the ozone and temperature structure of the stratosphere," J. Atmos. Sci., 30, pp. 667-675
- Reeger, E., and Seidentopf, F. 1946 "Die streufunktion des atmosphärischen dustes nach scheinwerfermessungen," Optik, 1, p. 15.
- Reiter, E. R. 1971 "Atmospheric transport processes, 2, Chemical tracers," Atomic Energy Comm., Oak Ridge, Tenn., 382 pp.
- Rosen, J. M. 1969 "Stratospheric dust and its relationship to the meteoric influx," Space Sci. Rev., 9, pp. 58-89.
- Rosen, J. M. 1971 "The boiling point of stratospheric aerosols," J. Appl. Meteor., 10, pp. 1044-1046.

- Russell, P. B., Viezee, W., and Hake, R. D., Jr. 1973a "Lidar measurements of the variability of stratospheric particulates," First Semiannual Report 2217, Contract NAS2-7261, Stanford Research Institute, Menlo Park, California.
- Russell, P. B., Viezee, W., and Hake, R. D., Jr. 1973b "Lidar measurements of the variability of stratospheric particulates," Second Semiannual Report 2217, Contract NAS2-7261, Stanford Research Institute, Menlo Park, California.
- Schuster, B. G. 1970 "Detection of tropospheric and stratospheric aerosol layers by optical radar (lidar)," J. Geophys. Res., 75, pp. 3123-3132.
- Schuster, B. G., Fernald, F. G., and Frush, C. L. 1973 "Global reconnaissance of stratospheric aerosol by airborne lidar," Fifth Conference on Laser Radar Studies of the Atmosphere, Williamsburg, Virginia, Conference Abstracts, p. 34.
- Sedlacek, William A., Los Alamos Scientific Laboratory, University of California, Los Alamos, New Mexico. 1973 Private communication.
- Spinhirne, J. D., Hansen, M. Z., and Reagan, J. A. 1973 "Monostatic lidar data recording and reduction system," Fifth Conference on Laser Radar Studies of the Atmosphere, Williamsburg, Virginia.
- Toon, O. B., and Pollack, J. B. 1973 "Physical properties of the stratospheric aerosols," J. Geophys. Res., 78, pp. 7051-7056.
- Viezee, W., Hake, R. D., and Russell, P. B. 1973 "Lidar measurements of stratospheric constituents," First Quarterly Report 2217, Contract NAS2-7261, Stanford Research Institute, Menlo Park, California.

- Volz, F. E. 1969 "Twilights and stratospheric dust before and after the Agung eruption," Appl. Opt., 8, pp. 2505-2517.
- Volz, F. E. 1970 "On dust in the tropical and mid-latitude stratosphere from recent twilight measurements," J. Geophys. Res., 75, pp. 1641-1646.
- Volz, F. E. 1971 "Stratospheric aerosol layers from balloonborne horizon photographs," Bull. Amer. Meteor. Soc., 52, pp. 996-998.
- Volz, F. E. 1972 "Return of normal stratospheric turbidity and a new short dust event during October, 1971," paper presented at International Radiation Symposium World Meteorol. Organ., Comm. for Space Res. ICSU, Amer. Meteorol. Soc., Meteorol. Soc. of Japan, Sendai, Japan.
- Volz, F. E. 1973 "The stratospheric dust event of October 1971," J. Geophysical Res., 79, 479-482.
- Wofsy, S. C., and McElroy, M. B. 1973 "On vertical mixing in the upper stratosphere and lower mesosphere," J. Geophysical Res., 78, pp. 2619-2624.
- Zakharov, V. M., Kostko, O. K., and Portasov, V. S. 1973 "The determination of tropospheric and lower mesospheric density, temperature and aerosol profile by a method of two-frequency laser sounding," paper presented at Fifth Conference on Laser Radar Studies of the Atmosphere, Williamsburg, Virginia, 4-6 June 1973.